EUROPEAN LABORATORY FOR PARTICLE PHYSICS

CERN-PPE/97-105
1 August 1997

Multiplicity distributions of gluon and quark jets and tests of QCD analytic predictions

The OPAL Collaboration

Abstract

Gluon jets are identified in e^+e^- hadronic annihilation events by tagging two quark jets in the same hemisphere of an event. The gluon jet is defined inclusively as all the particles in the opposite hemisphere. Gluon jets defined in this manner have a close correspondence to gluon jets as they are defined for analytic calculations, and are almost independent of a jet finding algorithm. The charged particle multiplicity distribution of the gluon jets is presented, and is analyzed for its mean, dispersion, skew, and curtosis values, and for its factorial and cumulant moments. The results are compared to the analogous results found for a sample of light quark (uds) jets, also defined inclusively. We observe differences between the mean, skew and curtosis values of gluon and quark jets, but not between their dispersions. The cumulant moment results are compared to the predictions of QCD analytic calculations. A calculation which includes next-to-next-to-leading order corrections and energy conservation is observed to provide a much improved description of the data compared to a next-to-leading order calculation without energy conservation. There is agreement between the data and calculations for the ratios of the cumulant moments between gluon and quark jets.

(To be submitted to Zeitschrift für Physik C)

The OPAL Collaboration

K. Ackerstaff[8], G. Alexander[23], J. Allison[16], N. Altekamp[5], K.J. Anderson[9], S. Anderson[12], S. Arcelli[2], S. Asai[24], D. Axen[29], G. Azuelos[18,a], A.H. Ball[17], E. Barberio[8], R.J. Barlow[16], R. Bartoldus[3], J.R. Batley[5], S. Baumann[3], J. Bechtluft[14], C. Beeston[16], T. Behnke[8], A.N. Bell[1], K.W. Bell[20], G. Bella[23], S. Bentvelsen[8], S. Bethke[14], O. Biebel[14], A. Biguzzi[5], S.D. Bird[16], V. Blobel[27], I.J. Bloodworth[1], J.E. Bloomer[1], M. Bobinski[10], P. Bock[11], D. Bonacorsi[2], M. Boutemeur[34], B.T. Bouwens[12], S. Braibant[12], L. Brigliadori[2], R.M. Brown[20], H.J. Burckhart[8], C. Burgard[8], R. Bürgin[10], P. Capiluppi[2], R.K. Carnegie[6], A.A. Carter[13], J.R. Carter[5], C.Y. Chang[17], D.G. Charlton[1,b], D. Chrisman[4], P.E.L. Clarke[15], I. Cohen[23], J.E. Conboy[15], O.C. Cooke[8], M. Cuffiani[2], S. Dado[22], C. Dallapiccola[17], G.M. Dallavalle[2], R. Davis[30], S. De Jong[12], L.A. del Pozo[4], K. Desch[3], B. Dienes[33,d], M.S. Dixit[7], E. do Couto e Silva[12], M. Doucet[18], E. Duchovni[26], G. Duckeck[34], I.P. Duerdoth[16], D. Eatough[16], J.E.G. Edwards[16], P.G. Estabrooks[6], H.G. Evans[9], M. Evans[13], F. Fabbri[2], M. Fanti[2], A.A. Faust[30], F. Fiedler[27], M. Fierro[2], H.M. Fischer[3], I. Fleck[8], R. Folman[26], D.G. Fong[17], M. Foucher[17], A. Fürtjes[8], D.I. Futyan[16], P. Gagnon[7], J.W. Gary[4], J. Gascon[18], S.M. Gascon-Shotkin[17], N.I. Geddes[20], C. Geich-Gimbel[3], T. Geralis[20], G. Giacomelli[2], P. Giacomelli[4], R. Giacomelli[2], V. Gibson[5], W.R. Gibson[13], D.M. Gingrich[30,a], D. Glenzinski[9], J. Goldberg[22], M.J. Goodrick[5], W. Gorn[4], C. Grandi[2], E. Gross[26], J. Grunhaus[23], M. Gruwé[8], C. Hajdu[32], G.G. Hanson[12], M. Hansroul[8], M. Hapke[13], C.K. Hargrove[7], P.A. Hart[9], C. Hartmann[3], M. Hauschild[8], C.M. Hawkes[5], R. Hawkings[27], R.J. Hemingway[6], M. Herndon[17], G. Herten[10], R.D. Heuer[8], M.D. Hildreth[8], J.C. Hill[5], S.J. Hillier[1], P.R. Hobson[25], R.J. Homer[1], A.K. Honma[28,a], D. Horváth[32,c], K.R. Hossain[30], R. Howard[29], P. Hüntemeyer[27], D.E. Hutchcroft[5], P. Igo-Kemenes[11], D.C. Imrie[25], M.R. Ingram[16], K. Ishii[24], A. Jawahery[17], P.W. Jeffreys[20], H. Jeremie[18], M. Jimack[1], A. Joly[18], C.R. Jones[5], G. Jones[16], M. Jones[6], U. Jost[11], P. Jovanovic[1], T.R. Junk[8], D. Karlen[6], V. Kartvelishvili[16], K. Kawagoe[24], T. Kawamoto[24], P.I. Kayal[30], R.K. Keeler[28], R.G. Kellogg[17], B.W. Kennedy[20], J. Kirk[29], A. Klier[26], S. Kluth[8], T. Kobayashi[24], M. Kobel[10], D.S. Koetke[6], T.P. Kokott[3], M. Kolrep[10], S. Komamiya[24], T. Kress[11], P. Krieger[6], J. von Krogh[11], P. Kyberd[13], G.D. Lafferty[16], R. Lahmann[17], W.P. Lai[19], D. Lanske[14], J. Lauber[15], S.R. Lautenschlager[31], J.G. Layter[4], D. Lazic[22], A.M. Lee[31], E. Lefebvre[18], D. Lellouch[26], J. Letts[12], L. Levinson[26], S.L. Lloyd[13], F.K. Loebinger[16], G.D. Long[28], M.J. Losty[7], J. Ludwig[10], A. Macchiolo[2], A. Macpherson[30], M. Mannelli[8], S. Marcellini[2], C. Markus[3], A.J. Martin[13], J.P. Martin[18], G. Martinez[17], T. Mashimo[24], P. Mättig[3], W.J. McDonald[30], J. McKenna[29], E.A. Mckigney[15], T.J. McMahon[1], R.A. McPherson[8], F. Meijers[8], S. Menke[3], F.S. Merritt[9], H. Mes[7], J. Meyer[27], A. Michelini[2], G. Mikenberg[26], D.J. Miller[15], A. Mincer[22,e], R. Mir[26], W. Mohr[10], A. Montanari[2], T. Mori[24], M. Morii[24], U. Müller[3], S. Mihara[24], K. Nagai[26], I. Nakamura[24], H.A. Neal[8], B. Nellen[3], R. Nisius[8], S.W. O'Neale[1], F.G. Oakham[7], F. Odorici[2], H.O. Ogren[12], A. Oh[27], N.J. Oldershaw[16], M.J. Oreglia[9], S. Orito[24], J. Pálinkás[33,d], G. Pásztor[32], J.R. Pater[16], G.N. Patrick[20], J. Patt[10], M.J. Pearce[1], R. Perez-Ochoa[8], S. Petzold[27], P. Pfeifenschneider[14], J.E. Pilcher[9], J. Pinfold[30], D.E. Plane[8], P. Poffenberger[28], B. Poli[2], A. Posthaus[3], D.L. Rees[1], D. Rigby[1], S. Robertson[28], S.A. Robins[22], N. Rodning[30], J.M. Roney[28], A. Rooke[15], E. Ros[8], A.M. Rossi[2], P. Routenburg[30], Y. Rozen[22], K. Runge[10], O. Runolfsson[8], U. Ruppel[14], D.R. Rust[12], R. Rylko[25], K. Sachs[10], T. Saeki[24], E.K.G. Sarkisyan[23], C. Sbarra[29], A.D. Schaile[34], O. Schaile[34], F. Scharf[3], P. Scharff-Hansen[8], P. Schenk[34], J. Schieck[11], P. Schleper[11], B. Schmitt[8], S. Schmitt[11], A. Schöning[8], M. Schröder[8], H.C. Schultz-Coulon[10], M. Schumacher[3], C. Schwick[8], W.G. Scott[20], T.G. Shears[16], B.C. Shen[4], C.H. Shepherd-Themistocleous[8], P. Sherwood[15], G.P. Siroli[2], A. Sittler[27], A. Skillman[15], A. Skuja[17], A.M. Smith[8], G.A. Snow[17], R. Sobie[28], S. Söldner-Rembold[10], R.W. Springer[30], M. Sproston[20], K. Stephens[16], J. Steuerer[27], B. Stockhausen[3], K. Stoll[10], D. Strom[19], P. Szymanski[20], R. Tafirout[18], S.D. Talbot[1], S. Tanaka[24], P. Taras[18], S. Tarem[22], R. Teuscher[8], M. Thiergen[10], M.A. Thomson[8], E. von Törne[3], S. Towers[6], I. Trigger[18], Z. Trócsányi[33], E. Tsur[23], A.S. Turcot[9], M.F. Turner-Watson[8], P. Utzat[11], R. Van Kooten[12], M. Verzocchi[10], P. Vikas[18], E.H. Vokurka[16], H. Voss[3], F. Wäckerle[10],

A. Wagner[27], C.P. Ward[5], D.R. Ward[5], P.M. Watkins[1], A.T. Watson[1], N.K. Watson[1], P.S. Wells[8], N. Wermes[3], J.S. White[28], B. Wilkens[10], G.W. Wilson[27], J.A. Wilson[1], G. Wolf[26], T.R. Wyatt[16], S. Yamashita[24], G. Yekutieli[26], V. Zacek[18], D. Zer-Zion[8]

[1]School of Physics and Space Research, University of Birmingham, Birmingham B15 2TT, UK
[2]Dipartimento di Fisica dell' Università di Bologna and INFN, I-40126 Bologna, Italy
[3]Physikalisches Institut, Universität Bonn, D-53115 Bonn, Germany
[4]Department of Physics, University of California, Riverside CA 92521, USA
[5]Cavendish Laboratory, Cambridge CB3 0HE, UK
[6] Ottawa-Carleton Institute for Physics, Department of Physics, Carleton University, Ottawa, Ontario K1S 5B6, Canada
[7]Centre for Research in Particle Physics, Carleton University, Ottawa, Ontario K1S 5B6, Canada
[8]CERN, European Organisation for Particle Physics, CH-1211 Geneva 23, Switzerland
[9]Enrico Fermi Institute and Department of Physics, University of Chicago, Chicago IL 60637, USA
[10]Fakultät für Physik, Albert Ludwigs Universität, D-79104 Freiburg, Germany
[11]Physikalisches Institut, Universität Heidelberg, D-69120 Heidelberg, Germany
[12]Indiana University, Department of Physics, Swain Hall West 117, Bloomington IN 47405, USA
[13]Queen Mary and Westfield College, University of London, London E1 4NS, UK
[14]Technische Hochschule Aachen, III Physikalisches Institut, Sommerfeldstrasse 26-28, D-52056 Aachen, Germany
[15]University College London, London WC1E 6BT, UK
[16]Department of Physics, Schuster Laboratory, The University, Manchester M13 9PL, UK
[17]Department of Physics, University of Maryland, College Park, MD 20742, USA
[18]Laboratoire de Physique Nucléaire, Université de Montréal, Montréal, Quebec H3C 3J7, Canada
[19]University of Oregon, Department of Physics, Eugene OR 97403, USA
[20]Rutherford Appleton Laboratory, Chilton, Didcot, Oxfordshire OX11 0QX, UK
[22]Department of Physics, Technion-Israel Institute of Technology, Haifa 32000, Israel
[23]Department of Physics and Astronomy, Tel Aviv University, Tel Aviv 69978, Israel
[24]International Centre for Elementary Particle Physics and Department of Physics, University of Tokyo, Tokyo 113, and Kobe University, Kobe 657, Japan
[25]Brunel University, Uxbridge, Middlesex UB8 3PH, UK
[26]Particle Physics Department, Weizmann Institute of Science, Rehovot 76100, Israel
[27]Universität Hamburg/DESY, II Institut für Experimental Physik, Notkestrasse 85, D-22607 Hamburg, Germany
[28]University of Victoria, Department of Physics, P O Box 3055, Victoria BC V8W 3P6, Canada
[29]University of British Columbia, Department of Physics, Vancouver BC V6T 1Z1, Canada
[30]University of Alberta, Department of Physics, Edmonton AB T6G 2J1, Canada
[31]Duke University, Dept of Physics, Durham, NC 27708-0305, USA
[32]Research Institute for Particle and Nuclear Physics, H-1525 Budapest, P O Box 49, Hungary
[33]Institute of Nuclear Research, H-4001 Debrecen, P O Box 51, Hungary
[34]Ludwigs-Maximilians-Universität München, Sektion Physik, Am Coulombwall 1, D-85748 Garching, Germany

[a] and at TRIUMF, Vancouver, Canada V6T 2A3
[b] and Royal Society University Research Fellow
[c] and Institute of Nuclear Research, Debrecen, Hungary
[d] and Department of Experimental Physics, Lajos Kossuth University, Debrecen, Hungary
[e] and Department of Physics, New York University, NY 1003, USA

1 Introduction

Many experimental studies of quark jets have been performed at e^+e^- colliders. Such studies are natural, since hadronic events in e^+e^- annihilations above the Υ region and below the threshold for W^+W^- production are believed to arise uniquely from the point-like creation of quark-antiquark $q\overline{q}$ pairs. Production of the $q\overline{q}$ pair from a color-singlet point source allows the quark jets to be defined inclusively, by sums over the particles in an event or the event hemispheres. In contrast, conclusive experimental studies of gluon jets have been rare. This is because the creation of a gluon jet pair, gg, from a color singlet point source – allowing an inclusive definition analogous to that described above for quark jets – has been only rarely observed in nature.[1] In most studies of gluon jets at e^+e^- colliders, a jet finding algorithm is used to select an exclusive sample of three-jet $q\overline{q}g$ events. The same jet finder is used to artificially divide the particles of an event into a gluon jet part and two quark jet parts. In general, the results depend strongly on the algorithm chosen. Furthermore, use of a jet finder precludes a quantitative test of QCD analytic predictions for gluon and quark jet properties. For the analytic calculations, the gluon and quark jet characteristics are given by inclusive sums over the particles in color singlet gg and $q\overline{q}$ events, respectively, as described above. Thus, the theoretical results are *not* restricted to three-jet events defined by a jet finder and do *not* employ a jet finder to assign particles to the jets.

In [2], a method was proposed for LEP experiments to identify gluon jets using an inclusive definition similar to that used for analytic calculations. The method is based on rare events of the type $e^+e^- \to q\overline{q}\,g_{\rm incl.}$, in which the q and $\overline{q}$ are identified quark (or antiquark) jets which appear in the same hemisphere of an event. The object $g_{\rm incl.}$, taken to be the gluon jet, is defined by the sum of all particles observed in the hemisphere opposite to that containing the q and $\overline{q}$. In the limit that the q and $\overline{q}$ are collinear, the gluon jet $g_{\rm incl.}$ is produced under the same conditions as gluon jets in gg events. The $g_{\rm incl.}$ jets therefore correspond closely to single gluon jets in gg events, defined by dividing the gg events in half using the plane perpendicular to the principal event axis. First experimental results using this method were presented in [3].

The results in [3] were limited to the mean charged particle multiplicity values of gluon and quark jets. In this paper, we extend this study to include the full multiplicity distributions. The data were collected using the OPAL detector at LEP. For the quark jet sample, we select light quark (uds) event hemispheres, as in [3]. Use of light quark events results in a better correspondence between the data and the massless quark assumption employed for analytic calculations, while use of event hemispheres to define the quark jets yields an inclusive definition analogous to that of the gluon jets $g_{\rm incl.}$. The multiplicity distributions of the gluon and quark jets are analyzed for their mean, dispersion, skew and curtosis values. In addition, we perform a factorial moment analysis of the gluon and quark jet multiplicity distributions in order to test the predictions of QCD analytic calculations [4, 5] of those moments.

[1] It is possible to identify a pure source of gg events in radiative Υ decays, such as in $\Upsilon(3S) \to \gamma\chi'_b$ followed by $\chi'_b \to gg$ [1]; however, the jet energies are only about 5 GeV in this case, which limits their usefulness for jet studies.

2 Detector and data sample

The OPAL detector is described in detail elsewhere [6]. The present analysis is based on a sample of about 3 708 000 hadronic Z^0 decay events collected by OPAL from 1991 to 1995. Charged tracks measured in the OPAL central detector and clusters of energy measured in the electromagnetic calorimeter were selected for the analysis using the criteria given in [7]. To minimize double counting of energy, clusters were used only if they were not associated with a charged track. Each accepted track and unassociated cluster was considered to be a particle. Tracks were assigned the pion mass. Clusters were assigned zero mass since they originate mostly from photons. To eliminate residual background and events in which a significant number of particles was lost near the beam direction, the number of accepted charged tracks was required to be at least five and the thrust axis [8] of the event, calculated using the particles, was required to satisfy $|\cos(\theta_{\rm thrust})| < 0.9$, where $\theta_{\rm thrust}$ is the angle between the thrust and beam axes. The residual background from all sources was estimated to be less than 1%.

3 Gluon jet selection

For this study, a gluon jet is defined inclusively by the particles observed in an e^+e^- event hemisphere opposite to a hemisphere containing an identified quark and antiquark jet, as stated in the introduction. The selection of inclusive gluon jets, $g_{\rm incl.}$, is performed using the technique presented in [3]. More details concerning the motivation for the selection choices are given there. To select the $g_{\rm incl.}$ gluon jets, each event is divided into hemispheres using the plane perpendicular to the thrust axis. Exactly two jets are reconstructed in each hemisphere, using the $k_\perp$ ("Durham") jet finder [9]. The results for the gluon jet properties are almost entirely insensitive to this choice of jet finder, as is discussed in [2] and below in sections 4 and 7.3. Next, we attempt to reconstruct a displaced secondary vertex in each of the four jets. Displaced secondary vertices are associated with heavy quark decay, especially that of the b quark. At LEP, b quarks are produced almost exclusively at the electroweak vertex: thus a jet containing a b hadron is almost always a quark jet. To identify secondary vertices in jets, we employ the method given in [10]. Briefly, a secondary vertex is required to contain at least three tracks, at least two of which have a signed impact parameter value in the r-ϕ plane[2] with respect to the primary event vertex, b, which satisfies $b/\sigma_b > 2.5$, with σ_b the error of b. For jets with such a secondary vertex, the signed decay length, L, is calculated with respect to the primary vertex, along with its error, σ_L. To be tagged as a quark jet, a jet is required to have a visible energy of at least 5 GeV and a successfully reconstructed secondary vertex with $L < 2.0$ cm and $L/\sigma_L > 3.5$.[3] The visible energy of a jet is defined by the sum of the energy of the particles assigned to the jet. We refer to a hemisphere with two tagged jets as a tagged hemisphere.

We next examine the angles that the two jets in a tagged hemisphere make with respect to the thrust axis and to each other. If the two jets are close together, or if one of the two jets is much more energetic than the other, it is very likely that one of the two jets is a gluon jet due to the strong kinematic similarity to an event with gluon radiation from a quark and because

[2] Our coordinate system is defined so that z is the coordinate parallel to the e^- beam axis, r is the coordinate normal to the beam axis, ϕ is the azimuthal angle around the beam axis and θ is the polar angle with respect to z.

[3] In [3], we utilized a more stringent requirement of $L/\sigma_L > 5.0$.

of the finite probability for a gluon jet to be identified as a b quark jet (see below). To reduce this background, we require the angle between the jets and thrust axis to exceed 10° and the angle between the two jets to exceed 50°. A last requirement is that the two jets lie no more than 70° from the thrust axis in order to eliminate jets near the hemisphere boundary. In total, 324 events are selected for the final gluon jet $g_{\rm incl.}$ sample.[4] There are no events in which both hemispheres are tagged.

We estimate the purity of this sample using the Jetset parton shower Monte Carlo [11], including detector simulation [12] and the same analysis procedures as are applied to the data. The Jetset sample is a combination of events generated using version 7.3 of the program with the parameter values given in [13] and of events generated using version 7.4 of the program with the parameter values given in [7]. The initial Monte Carlo samples have about 3 000 000 events for version 7.3 and 4 000 000 events for version 7.4. The two Jetset versions yield results which are consistent with each other to within the statistical uncertainties and so we combine them. Using the Jetset events, the hadron level jets are examined to determine whether they are associated with an underlying quark or antiquark jet. To perform this association, the Monte Carlo events are also examined at the parton level. We determine the directions of the primary quark or antiquark from the Z^0 decay after the parton shower evolution has terminated. The hadron jet closest to the direction of an evolved primary quark or antiquark is considered to be a quark jet. The distinct hadron jet closest to the evolved primary quark or antiquark not associated with this first hadron jet is considered to be the other quark jet. With the final cuts, Jetset predicts that both jets in the tagged hemisphere are quark jets with $(80.5 \pm 1.6)\%$ probability, where the uncertainty is statistical: this is the estimated purity of the $g_{\rm incl.}$ gluon jet sample. As an alternative method to estimate the gluon jet purity, we determine the fraction of events in the Monte Carlo $g_{\rm incl.}$ sample for which the evolved primary quark and antiquark are both in the hemisphere opposite the $g_{\rm incl.}$ jet: this yields the same estimate as given above. The Monte Carlo predicts that about 80% of the background is comprised of b events in which a gluon jet is mistakenly tagged as a b jet, while the other 20% is comprised about evenly of u, d, s and c events in which both a quark jet and a gluon jet are mistakenly tagged as b jets. The background events occur mostly when two tracks from the decay of a Λ or K^0_S hadron are combined with a third track to define a secondary vertex.

Because we rely on displaced secondary vertices to identify quark jets, the $g_{\rm incl.}$ jets in our study are contained in heavy quark events. The Monte Carlo with detector simulation predicts that about 95% of the events in the $g_{\rm incl.}$ sample are b events. This reliance on b events is not expected to affect our results since the properties of hard, acollinear gluon jets do not depend on the event flavor according to QCD. More details are given in [3].

We note that the $g_{\rm incl.}$ jet tag rate, defined by the ratio of the number of $g_{\rm incl.}$ jets to the number of events in the initial inclusive multihadronic event sample, is $(8.74 \pm 0.49\,(\text{stat.})) \times 10^{-5}$ for the data and $(8.83 \pm 0.36\,(\text{stat.})) \times 10^{-5}$ for the Monte Carlo. Thus the Monte Carlo reproduces the measured tag rate well.

The mean energy of the gluon jets, $\langle E \rangle_{g_{\rm incl.}}$, is less than the beam energy because the two quark jets against which $g_{\rm incl.}$ recoils are not entirely collinear. The mean visible energy

[4] Because we use a somewhat different event selection here, and because our data have been reprocessed using improved detector calibrations since the time of our previous publication [3], only 60% of these events are in common with the $g_{\rm incl.}$ sample in [3].

of the $g_{\rm incl.}$ jets, corrected for the effects of the detector and initial-state photon radiation, is 41.8 ± 0.6 (stat.) GeV. As an alternative method to estimate the gluon jet energy, we employ the technique of calculated jet energies for massive jets. A jet direction is determined for the gluon jet by summing the momenta of the particles in the $g_{\rm incl.}$ hemisphere. The angles between the $g_{\rm incl.}$ jet and the two jets in the tagged hemisphere are used in conjunction with the measured jet velocities to calculate the jet energies assuming energy-momentum conservation.[5] The velocity of a jet is given by the magnitude of its visible 3-momentum divided by its visible energy. Using this method, the mean gluon jet energy is determined to be 41.5 ± 0.3 (stat.) GeV, which is consistent with the result given above for the visible energy. In this paper, we choose to use the visible $g_{\rm incl.}$ energy, rather than the calculated energy, because it corresponds more closely to the jet energy as it is defined for the uds hemisphere quark jets. The difference between the mean visible and calculated jet energies is used to define a systematic uncertainty. The mean energy of the gluon jets in our study is therefore $\langle E \rangle_{g_{\rm incl.}} = 41.8 \pm 0.6\,({\rm stat.}) \pm 0.3\,({\rm syst.})$ GeV.

4 Monte Carlo comparison of $g_{\rm incl.}$ and gg jets

Our analysis of gluon jets is based on the premise that $g_{\rm incl.}$ jets from e^+e^- annihilations are equivalent to hemispheres of gg events produced from a color singlet point source, with the hemispheres defined by the plane perpendicular to the thrust axis. Although high energy gg events are not available experimentally, they may be generated using a QCD Monte Carlo event generator. The viability of our premise can be tested by comparing the Monte Carlo predictions for gg event hemispheres and $g_{\rm incl.}$ jets. Such a comparison has already been presented in [2] for the mean charged particle multiplicity values, $\langle n_{\rm ch.} \rangle$ (see also [14]). Here, we extend this comparison to the full multiplicity distribution, $P(n_{\rm ch.})$ versus $n_{\rm ch.}$, with $P(n_{\rm ch.})$ the probability that an event will be observed with a charged particle multiplicity $n_{\rm ch.}$.

The points with error bars in Figure 1 show the prediction of the Herwig parton shower Monte Carlo [15], version 5.9, for the charged particle multiplicity distribution of $g_{\rm incl.}$ jets. The uncertainties are statistical. The parameter set we use is the same as that given in [7] for Herwig, version 5.8, except that the value of the cluster mass cutoff CLMAX has been increased from 3.40 GeV/c^2 to 3.75 GeV/c^2 to improve the model's description of $\langle n_{\rm ch.} \rangle$ in inclusive hadronic Z^0 decays. The $e^+e^- \to q\overline{q}\,g_{\rm incl.}$ events were generated using a center-of-mass (c.m.) energy, $E_{\rm c.m.}$, of 91.2 GeV to correspond to the data. The $g_{\rm incl.}$ identification was performed using the same procedure as is described for the data in section 3, except that the two quark jets against which the $g_{\rm incl.}$ jet recoils were identified using the Monte Carlo method described in section 3. In particular, the angular cuts on the directions of the quark jets with respect to the thrust axis and to each other have been applied. The resulting mean energy of the Monte Carlo $g_{\rm incl.}$ jets is 41.2 GeV with a negligible statistical uncertainty.

Shown by the solid histogram in Figure 1 is the prediction of Herwig for gg event hemispheres. The gg events were generated using a c.m. energy of 82.4 GeV so that the hemisphere energies are the same as for the $g_{\rm incl.}$ jets. It is seen that the results for the $g_{\rm incl.}$ jets and the gg

[5] This method results in a better estimate of the $g_{\rm incl.}$ jet energy than the method assuming massless jets which we employed in [3]: the Monte Carlo without detector simulation yields identical results for the visible and calculated $g_{\rm incl.}$ jet energies if the massive formula is used, whereas the calculated energy is about 2 GeV smaller than the visible one if the massless formula is used.

event hemispheres are essentially identical. This establishes the viability of our method, confirming the results of [2]. Similar agreement between the predicted multiplicity distributions of $g_{\rm incl.}$ jets and gg event hemispheres is obtained if Jetset is used to generate the samples rather than Herwig, or if the JADE-E0 [16] or cone [17] jet finder is used to identify the quark jets for the $g_{\rm incl.}$ jet selection, rather than the $k_\perp$ jet finder.

5 uds quark jet selection

The uds quark jets in our study are defined inclusively, by summing the particles observed in an event hemisphere opposite to a hemisphere containing an identified uds jet. Since there are only 324 gluon jets in our study, it is not necessary to use the entire data sample of about 3 708 000 events mentioned in section 2 for the uds jet analysis. Instead, we base the uds jet selection on an initial sample of about 396 000 hadronic annihilation events with c.m. energies within 100 MeV of the Z^0 peak.

To select the uds jets, we divide each event into hemispheres using the plane perpendicular to the thrust axis. Selection criteria are applied to each hemisphere separately using charged tracks that appear in a cone of half angle 40° around the thrust axis. The reason for the restriction to tracks which lie within 40° of the thrust axis is to avoid using tracks near the hemisphere boundary. An algorithm is applied to identify charged tracks which are consistent with arising from photon conversions [18]. Removing such tracks from consideration, the number of tracks in the cone which have a signed impact parameter significance, b/σ_b, greater than 1.5 is determined. A hemisphere is tagged as containing a uds jet if the number of tracks in the cone which have $b/\sigma_b > 1.5$ is zero. In total, 188 288 hemispheres are tagged. This number includes 30 303 events for which both hemispheres are tagged. The estimated uds purity of this sample, obtained by treating Jetset events with detector simulation in the same manner as the data, is 80.9%, with a negligible statistical uncertainty. The Monte Carlo predicts that about 70% of the background events are c events and that 30% are b events. The uds jet tag rate, defined by the ratio of the number of tagged uds jets to the number of events in the initial inclusive multihadronic event sample, is 0.399 ± 0.001 (stat.) for the data and 0.418 ± 0.001 (stat.) for the Monte Carlo. The difference of about 2% between the uds jet tag rates of data and Monte Carlo implies a small deficiency in the simulation of the event characteristics, which is accounted for in our evaluation of systematic uncertainties (section 7.3). The corrected energy of the uds jets is given by the beam energy, 45.6 GeV, with essentially no uncertainty.

For purposes of comparison, Figure 1 includes the prediction of Herwig for uds $q\overline{q}$ event hemispheres, generated using the same c.m. energy that is used to generate the gg event sample.

6 Corrections

The measured charged particle multiplicity distributions of the $g_{\rm incl.}$ and uds jets are corrected in two steps, following the method presented in [19]. In the first step, the data are corrected for experimental acceptance, resolution, and secondary electromagnetic and hadronic interactions

using an unfolding matrix [19]. This matrix is constructed using Jetset events, including full detector simulation and the same selection criteria as are applied to the data. In the second step, the data are corrected for event acceptance and the effects of initial-state photon radiation using bin-by-bin multiplicative factors. The bin-by-bin corrections are derived using two different Jetset samples. The first sample, based on inclusive Z^0 hadronic decays, includes initial-state photon radiation and the same event acceptance criteria as the data, but not detector simulation (they are the generator level input to events which have been processed through the detector simulation and which have been selected using the same selection criteria as are applied to the data). The second sample does not include initial-state photon radiation, event acceptance, or detector simulation and treats all charged and neutral particles with mean lifetimes greater than 3×10^{-10} s as stable: hence charged particles from the decays of K^0_S and weakly decaying hyperons are included in the definition of multiplicity. For the correction of the gluon jet data, inclusive Z^0 events are used for the second sample. The quark jets in this sample are identified with Monte Carlo information using the method discussed in section 3: otherwise the $g_{\rm incl.}$ sample is obtained in the same manner as is described in section 3 for the data. For the correction of the uds jet data, the jets of the second sample are defined by the particles in the hemispheres of uds events. The multiplicative correction factors are obtained by taking the ratios of the predictions from the second sample to those from the first one. Thus, the bin-by-bin corrections account not only for detector response and initial-state radiation but also for the background to the $g_{\rm incl.}$ and uds jet data. The corrections applied to the data are generally moderate or small. For example, Jetset predicts the mean multiplicity value (section 7.1) of $g_{\rm incl.}$ jets to be only 6% larger at the generator level than it is at the level which includes detector simulation and the experimental selection criteria. The corresponding difference for uds jets is -4%.

7 Results

The corrected charged particle multiplicity distributions are presented in Figure 2. Numerical values for these data are listed in Table 1. Shown in comparison to the data are the generator level predictions of Herwig 5.9 and Jetset 7.4. The Monte Carlo results for the $g_{\rm incl.}$ jets are obtained in the manner described in section 4. The two models are seen to provide a generally adequate description of the measurements except that the uds jet distribution predicted by Herwig is shifted towards lower values of multiplicity than are observed experimentally (Figure 2(b)). Statistical uncertainties were estimated for the $g_{\rm incl.}$ results using 100 Monte Carlo samples of $g_{\rm incl.}$ jets at the generator level, each with approximately the same event statistics as the data sample. The statistical uncertainty for each result (e.g. a multiplicity bin in Figure 2(a) or a factorial moment measurement, see section 7.2) was set equal to the RMS value found for the 100 samples. The same method was used to evaluate statistical uncertainties for the uds jets. The matrix corrections introduce correlations between the bins of the corrected multiplicity distributions. The correlations are generally strong between a bin and its nearest one or two neighbors on either side but can extend with smaller strength to four or five bins away. These correlations smooth out bin-to-bin statistical fluctuations. This effect is particularly noticeable for the gluon jet distribution (Figure 2(a)) because of the relatively small number of events in the $g_{\rm incl.}$ jet sample.

7.1 Mean, dispersion, skew and curtosis values

We determine the mean $\langle n_{\rm ch.}\rangle$, dispersion $D \equiv \sqrt{\langle n_{\rm ch.}^2\rangle - \langle n_{\rm ch.}\rangle^2}$, skew $\gamma \equiv \langle (n_{\rm ch.} - \langle n_{\rm ch.}\rangle)^3\rangle / D^3$ and curtosis $c \equiv [(\langle (n_{\rm ch.} - \langle n_{\rm ch.}\rangle)^4\rangle / D^4) - 3]$ values of 41.8 GeV $\rm g_{incl.}$ gluon jet and 45.6 GeV uds quark jet hemispheres to be:

$$\begin{aligned}
\langle n_{\rm ch.}\rangle_{\rm g_{incl.}} &= 14.32 \pm 0.23 \pm 0.40 \qquad (1)\\
\langle n_{\rm ch.}\rangle_{\rm uds\,hemis.} &= 10.10 \pm 0.01 \pm 0.18 \\
D_{\rm g_{incl.}} &= 4.37 \pm 0.19 \pm 0.26 \qquad (2)\\
D_{\rm uds\,hemis.} &= 4.298 \pm 0.008 \pm 0.098 \\
\gamma_{\rm g_{incl.}} &= 0.38 \pm 0.13 \pm 0.18 \qquad (3)\\
\gamma_{\rm uds\,hemis.} &= 0.822 \pm 0.007 \pm 0.044 \\
c_{\rm g_{incl.}} &= 0.18 \pm 0.34 \pm 0.30 \qquad (4)\\
c_{\rm uds\,hemis.} &= 0.98 \pm 0.03 \pm 0.11 \quad ,
\end{aligned}$$

where the first uncertainty is statistical and the second is systematic. These results are shown in Figures 3 and 4. The systematic uncertainties are discussed below in section 7.3. The results for $\langle n_{\rm ch.}\rangle_{\rm g_{incl.}}$ and $\langle n_{\rm ch.}\rangle_{\rm uds\,hemis.}$ are consistent with those presented in [3, 20].

Figures 3 and 4 include the Herwig and Jetset predictions for $\rm g_{incl.}$ jets, shown by the cross and diamond symbols, respectively. Also shown, by the finely-dashed and solid horizontal lines, are the Monte Carlo predictions for gg event hemispheres, generated to have the same energy as the $\rm g_{incl.}$ jets. It is seen that the results for the gg hemispheres and $\rm g_{incl.}$ samples agree well for both Herwig and Jetset (compare the cross symbols to the finely-dashed lines and the diamond symbols to the solid lines), which is consistent with Figure 1 and the discussion in section 4. The Monte Carlo predictions for gluon jet properties are seen to agree well with the data, except that the Jetset prediction of the mean multiplicity $\langle n_{\rm ch.}\rangle_{\rm g_{incl.}}$ is somewhat above the measured value (Figure 3(a)).

Also shown in Figures 3 and 4, by the coarsely-dashed and dash-dotted horizontal lines, are the predictions of Herwig and Jetset for uds event hemispheres. These predictions are shown for two different values of jet energy: $E_{\rm jet}$=45.6 GeV ($E_{\rm c.m.}$=91.2 GeV), corresponding to the energy of the measured uds jets, and $E_{\rm jet}$=41.8 GeV ($E_{\rm c.m.}$=83.6 GeV), corresponding to the energy of the $\rm g_{incl.}$ jets. The steps in Figures 3 and 4 between the predictions for $E_{\rm c.m.}$=91.2 GeV and $E_{\rm c.m.}$=83.6 GeV uds hemispheres therefore indicate the Monte Carlo corrections for quark jets to account for the difference in energy between the uds and $\rm g_{incl.}$ samples. Comparing the Monte Carlo predictions for $E_{\rm c.m.}$=91.2 GeV to the data, it is seen that Jetset provides a good overall description of the uds jet properties. Herwig's predictions for the uds jet properties are also in reasonable agreement with the data, with the exception of the mean multiplicity $\langle n_{\rm ch.}\rangle_{\rm uds\,hemis.}$ (Figure 3(a)), which is somewhat too low as was already noted in connection with Figure 2(b).

We also determine the ratios between the gluon and quark jet results since common systematic uncertainties will partially cancel. Before forming these ratios, it is necessary to account for the different energies of the two samples: the gluon jets have a mean energy of 41.8 GeV

while the uds jets have a mean energy of 45.6 GeV. To correct the quark jet $\langle n_{\rm ch.}\rangle$ value for this difference in energy, we follow the method in [3] and employ the QCD analytic formula for the evolution of the mean event multiplicity in e^+e^- annihilations [21]. This QCD result is known to describe the energy evolution of the mean charged particle multiplicity in inclusive e^+e^- annihilation events with good accuracy [22]. Assuming the number of active quark flavors, n_f, to be five, the QCD evolution formula predicts the mean multiplicity of 41.8 GeV quark jet hemispheres to be $(3.6 \pm 0.2)\%$ smaller than for 45.6 GeV quark jet hemispheres, where the uncertainty results from the maximum variation found by using the jet energies (41.8 GeV and 45.6 GeV) rather than the event energies (83.6 GeV and 91.2 GeV), n_f=3 rather than n_f=5, and varying the value of $\Lambda_{\overline{\rm MS}}$ within its allowed range [23].[6] Virtually the same result is obtained if the evolution formula is evaluated using the fitted values given in [24] for the strong coupling strength and the overall normalization. Applying a multiplicative correction of 0.964 to the result presented above for $\langle n_{\rm ch.}\rangle_{\rm uds\,hemis.}$ yields $\langle n_{\rm ch.}\rangle^{41.8\,\rm GeV}_{\rm uds\,hemis.}=9.74 \pm 0.01\,(\rm stat.)$. Our result for the multiplicity ratio $r_{\rm ch.}$ between 41.8 GeV gluon and quark jets is therefore:

$$r_{\rm ch.} \equiv \frac{\langle n_{\rm ch.}\rangle_{\rm g_{incl.}}}{\langle n_{\rm ch.}\rangle^{41.8\,\rm GeV}_{\rm uds\ hemis.}} = 1.471 \pm 0.024\,(\rm stat.) \pm 0.043\,(\rm syst.) \quad . \tag{5}$$

This result is consistent with our previous result [3],[7] but has substantially reduced uncertainties. Furthermore, the analytic prediction in [25] is in general agreement with this measurement. For purposes of comparison, the predictions of Herwig and Jetset are $r_{\rm ch.}$=1.537 ± 0.002 and 1.539 ± 0.002, respectively, where the uncertainties are statistical.

For the dispersion, skew and curtosis values, we account for the difference in energy between the gluon and quark jet measurements using the Monte Carlo predictions. The Monte Carlo is known to provide a good description of the energy evolution of the dispersion of the multiplicity distribution in inclusive e^+e^- hadronic events (e.g. see [19, 22, 24]), making it plausible that its predictions for the energy evolution of skew and curtosis are also reliable. Jetset predicts the dispersion D to be $(3.6 \pm 0.2)\%$ smaller for 41.8 GeV uds hemispheres than for 45.6 GeV uds hemispheres (Figure 3(b)). The corresponding results for skew and curtosis are $(2.5 \pm 0.5)\%$ and $(4.5 \pm 2.2)\%$, respectively (Figure 4(a) and (b)). The uncertainties for these values are given by the maximum variation found by using Herwig rather than Jetset, n_f=5 rather than n_f=3, and varying the value of $\Lambda_{\rm LLA}$ by its uncertainty [7]. Applying corrections of 0.964, 0.975 and 0.955 to the uds jet dispersion, skew and curtosis measurements given above, respectively, yields $D^{41.8\,\rm GeV}_{\rm uds\,hemis.} = 4.143 \pm 0.008\,(\rm stat.)$, $\gamma^{41.8\,\rm GeV}_{\rm uds\,hemis.} = 0.802 \pm 0.007\,(\rm stat.)$, and $c^{41.8\,\rm GeV}_{\rm uds\,hemis.} = 0.933 \pm 0.027\,(\rm stat.)$. The ratios between the dispersion, skew and curtosis values of 41.8 GeV gluon and quark jets are therefore:

$$r_D \equiv \frac{D_{\rm g_{incl.}}}{D^{41.8\,\rm GeV}_{\rm uds\ hemis.}} = 1.055 \pm 0.046\,(\rm stat.) \pm 0.055\,(\rm syst.) \tag{6}$$

$$r_\gamma \equiv \frac{\gamma_{\rm g_{incl.}}}{\gamma^{41.8\,\rm GeV}_{\rm uds\ hemis.}} = 0.47 \pm 0.16\,(\rm stat.) \pm 0.21\,(\rm syst.) \tag{7}$$

$$r_c \equiv \frac{c_{\rm g_{incl.}}}{c^{41.8\,\rm GeV}_{\rm uds\ hemis.}} = 0.19 \pm 0.37\,(\rm stat.) \pm 0.33\,(\rm syst.) \quad . \tag{8}$$

[6] Jetset and Herwig predict reductions of 3.5% and 3.6%, respectively, in the value of $\langle n_{\rm ch.}\rangle$ for uds hemispheres with $E_{\rm c.m.}$=83.6 GeV compared to those with $E_{\rm c.m.}$=91.2 GeV: thus the Monte Carlo predictions for the energy correction are essentially the same as that obtained from the QCD evolution formula.

[7] There is a shift of 0.081 between the central values of our previous result ($r_{\rm ch.}=1.552 \pm 0.073$ (stat.+syst.)) and our current result; this shift is due primarily to our reevaluation of the $\rm g_{incl.}$ energy value (section 3) and thus to a reevaluation of the correction to account for the difference in energy between the uds and $\rm g_{incl.}$ jets.

The dispersions of the gluon and quark jet multiplicity distributions are therefore almost equal, despite the large difference between their mean values (relation (5)). The quark jet distribution is more skewed, i.e. asymmetric, than the corresponding distribution for gluon jets. Quark jets are observed to have a larger curtosis value than gluon jets, implying that their distribution is more non-gaussian in shape (the peak is higher and the tails are broader than a gaussian with the same mean and dispersion) than is the case for gluon jets. We note that the deviations of the ratios r_γ and r_c from unity are only 2.0 and 1.6 standard deviations of their total uncertainties, however. Herwig predicts r_D=1.086 $\pm$ 0.003, r_γ=0.60 $\pm$ 0.01 and r_c=0.30 $\pm$ 0.03, where the uncertainties are statistical. The corresponding results from Jetset are 1.110 $\pm$0.003, 0.55 $\pm$ 0.01 and 0.31 $\pm$ 0.03.

7.2 Factorial, cumulant and H_q moments

Factorial moments provide a standard means to characterize the fluctuations of a distribution about its mean value (cf. [4, 5, 26]). Factorial moments are less subject to bias from random statistical fluctuations than "ordinary" central moments, as is discussed in [26]. Various QCD analytic calculations have been performed for the factorial moments of the multiplicity distributions of separated gluon and quark jets [4, 5]. A factorial moment analysis of our data permits a test of these QCD calculations for the first time (see section 8). Currently, QCD predictions do not exist for the dispersion, skew and curtosis values presented in section 7.1. Certain combinations of factorial moments are directly related to these three quantities, however, as is discussed below.

The normalized factorial moment of rank q, F_q, is defined by [26, 27]:

$$F_q \equiv \frac{\langle n\,(n-1)\cdots(n-q+1)\rangle}{\langle n\rangle^q} \quad , \tag{9}$$

where $q \geq 1$. An equivalent characterization is given by the cumulant factorial moments, K_q [27], which can be obtained from the F_q moments recursively:

$$K_q \equiv F_q - \sum_{m=1}^{q-1} \frac{(q-1)!}{m!(q-m-1)!}\, K_{q-m}\, F_m \quad , \tag{10}$$

with the condition K_1=1. The K_q moments have been shown to be more sensitive to detailed features of the multiplicity distribution than the F_q moments [27]: they are more sensitive to higher order QCD corrections and to differences between QCD and phenomenological parametrizations such as the negative binomial distribution. Besides factorial and cumulant moments, it has become standard to consider the ratio of cumulant to factorial moments, denoted H_q, which appear naturally in the solution of the QCD equations [28]:

$$H_q \equiv \frac{K_q}{F_q} \quad . \tag{11}$$

An analysis of the H_q factorial moments of the inclusive multiplicity distribution in multihadronic Z^0 decays has recently been presented in [29, 30].

In Tables 2 and 3, we present our measurements of the F_q, K_q and H_q factorial moments of $g_{\text{incl.}}$ and uds jets. Our results are given for ranks $2 \leq q \leq 5$. (F_1=K_1=H_1=1 trivially.) These

ranks correspond to those for which theoretical predictions have been published [4, 5]. The results for F_q and K_q are shown in Figures 5 and 6. The results for H_q are qualitatively similar to those shown in Figure 6 for K_q and so are not shown in addition. Figures 5 and 6 include the predictions of Herwig and Jetset. The Monte Carlo information is presented in the same manner as in Figures 3 and 4. It is seen that the Monte Carlo results for the $g_{\rm incl.}$ and gg event hemispheres agree well with each other, i.e. the cross symbols agree with the finely-dashed lines and the diamond symbols agree with the solid lines to within differences that are consistent with statistical fluctuations. It is also seen that the Monte Carlo corrections to uds jets to account for the difference in energy between the $g_{\rm incl.}$ and uds samples (the steps in the center of the coarsely-dashed and dash-dotted curves in Figures 5 and 6) are moderate in comparison to the experimental uncertainties.

To gain insight concerning the physical interpretation of the factorial and cumulant moments, and to help relate the measurements shown in Figures 5 and 6 to those shown in Figures 3 and 4, we generated 100 samples of $g_{\rm incl.}$ jets using the Jetset Monte Carlo, each with event statistics similar to that of the data. We used these 100 generator level samples to calculate the correlation coefficients between the F_q moments, the K_q moments and the mean, dispersion, skew and curtosis values. The resulting correlation matrix is presented in Table 4. Similar results were found in an analogous study of uds quark jets. We also selected 24 independent samples of uds events which included detector simulation and the same selection criteria as the data. We processed these 24 samples using the correction procedure described in section 6 and determined the correlations between the corrected results. The detector level study was not repeated for $g_{\rm incl.}$ jets because of inadequate Monte Carlo event statistics. The resulting correlation matrix (corresponding to Table 4) was found to be very similar to that obtained using the 100 generator level samples, from which we conclude that the correction procedure does not introduce significant correlations between the variables. To facilitate the discussion in the next paragraph, boxes have been drawn around correlation coefficients in Table 4 which have magnitudes of 0.90 or larger.

From Table 4, it is seen that there is a high degree of statistical correlation between factorial moments of different rank: the correlation coefficients between the various F_q moments lie between 0.92 and 0.99. In contrast, only modest or small correlations are observed between the cumulant moments. The largest correlation coefficient in this case, between the K_q moments with ranks q=3 and q=4, is only 0.43. Thus, the results shown for different ranks in Figure 6 are largely independent of each other, while those shown in Figure 5 are not. Table 4 also establishes that the cumulant moments of ranks 2, 3 and 4 are strongly correlated with dispersion, skew and curtosis, respectively (correlation coefficients of 0.97, 0.99 and 0.90). Furthermore, with the exception of the correlation between K_3 and curtosis (coefficient of 0.78), the other correlations of the cumulant moments with dispersion, skew and curtosis are moderate or small. Therefore, the cumulant moments of ranks 2, 3 and 4 are directly related to dispersion, skew and curtosis, respectively. Algebraically, the relationships are:

$$K_2 = \left(\frac{D}{\langle n_{\rm ch.}\rangle}\right)^2 - \frac{1}{\langle n_{\rm ch.}\rangle} \tag{12}$$

$$K_3 = \gamma\left(\frac{D}{\langle n_{\rm ch.}\rangle}\right)^3 - \frac{3}{\langle n_{\rm ch.}\rangle}\left(\frac{D}{\langle n_{\rm ch.}\rangle}\right)^2 + \frac{2}{\langle n_{\rm ch.}\rangle^2} \tag{13}$$

$$K_4 \;=\; c\left(\frac{D}{\langle n_{\,\mathrm{ch.}}\rangle}\right)^4 - \frac{6\gamma}{\langle n_{\,\mathrm{ch.}}\rangle}\left(\frac{D}{\langle n_{\,\mathrm{ch.}}\rangle}\right)^3 + \frac{11}{\langle n_{\,\mathrm{ch.}}\rangle^2}\left(\frac{D}{\langle n_{\,\mathrm{ch.}}\rangle}\right)^2 - \frac{6}{\langle n_{\,\mathrm{ch.}}\rangle^3} \quad . \qquad (14)$$

Thus, the K_q moments with q=2, 3 and 4 are essentially equivalent to dispersion, skew and curtosis, but are in a form for which QCD analytic calculations have been presented (see section 8). In contrast, the F_q moments exhibit a strong correlation with dispersion but not with skew or curtosis, as is seen from Table 4.

In Table 5, we present measurements of the ratios r_{F_q}, r_{K_q} and r_{H_q} between the F_q, K_q and H_q factorial moments of 41.8 GeV gluon and quark jets. To obtain these results, the quark jet values in Table 3 were corrected for the difference in energy between the uds and $\mathrm{g_{incl.}}$ samples using the method described in section 7.1 for the dispersion, skew and curtosis, i.e. using the Jetset predictions (e.g. Figures 5 and 6), with a systematic uncertainty evaluated as is described in section 7.1. These corrections typically lie between 0.95 and 0.99. The ratios r_{F_q}, r_{K_q} and r_{H_q} are then formed by dividing the factorial moments of gluon jets (Table 2) by these corrected quark jet results. Our measurements of the cumulant moment ratios r_{K_q} are shown in Figure 7. It is seen that the gluon and quark jet cumulant moments differ by about a factor of three for q=2 and by an even larger amount for the higher moments. From relations (12)-(14), it is seen that part of this difference can be attributed to the difference between the mean values $\langle n_{\,\mathrm{ch.}}\rangle$ of gluon and quark jets (relation (5)). The results are well reproduced by the predictions of Herwig and Jetset, shown by the dashed and solid horizontal lines in Figure 7.

7.3 Systematic Uncertainties

To evaluate systematic uncertainties, the analysis was repeated with the following changes relative to the standard analysis. There were no significant changes in the number of selected events or in their estimated purities compared to the standard results unless otherwise noted.

1. Charged tracks alone were used for the data and for the Monte Carlo samples which include detector simulation, rather than charged tracks plus unassociated electromagnetic clusters.

2. Herwig was used to determine the correction matrix and bin-by-bin correction factors, rather than Jetset.

3. The particle selection was varied, first by restricting charged tracks and electromagnetic clusters to the central region of the detector, $|\cos(\theta)| < 0.70$, rather than $|\cos(\theta)| < 0.94$ for the charged tracks and $|\cos(\theta)| < 0.98$ for the clusters, and second by increasing the minimum momentum of charged tracks, $p^{\mathrm{ch.}}_{\mathrm{min.}}$, from 0.10 GeV/$c$ to 0.20 GeV/c.

4. The gluon jet selection was performed using the JADE-E0 [16] and cone [17] jet finders to define the tagged quark jets, rather than the $k_\perp$ jet finder: 320 and 246 $\mathrm{g_{incl.}}$ jets resulted, respectively, of which 88% and 76% were in common with the events of the standard $\mathrm{g_{incl.}}$ sample.

5. The geometric conditions for the gluon jet selection were varied, first by requiring the angle between the two jets in the tagged hemisphere to exceed 65°, rather than 50°, and

second by requiring the two tagged quark jets to lie within 65° of the thrust axis, rather than 70°.

6. At least one track with a signed impact parameter significance greater than 2.5 was required to be present in the displaced secondary vertices used to tag quark jets for the $g_{\rm incl.}$ identification, rather than at least two; the $g_{\rm incl.}$ sample increased to 1127 jets, while its estimated gluon jet purity decreased to 55.8%.

7. The gluon jet sample was restricted to events collected within 100 MeV of the Z^0 peak.

8. uds jets were tagged using charged tracks that appeared within a cone of half angle 70° around the thrust axis, rather than 40°.

9. The maximum signed impact parameter significance of tracks used for the identification of uds jets was increased from 1.5 to 2.5.

10. For the ratios of mean multiplicity, dispersion, skew and curtosis $r_{\rm ch.}$, r_D, r_γ and r_c, and for the ratios of factorial moments r_{F_q}, r_{K_q} and r_{H_q}, the energy to which the quark jet results were corrected was varied by the total uncertainty of the $g_{\rm incl.}$ jet energy (section 3); also, for these same quantities, the correction factors to account for the difference between the uds and $g_{\rm incl.}$ jet energies were varied by their uncertainties (sections 7.1 and 7.2).

The differences between the standard results and those found using each of these conditions were used to define symmetric systematic uncertainties. For items 3, 4, 5 and 10, the larger of the two described differences with respect to the standard result was assigned as the systematic uncertainty. For item 2, the difference with respect to the standard result was multiplied by $2/\sqrt{12}$ [31] since Herwig represents an extreme choice of hadronization model compared to Jetset. For the uds jet differential multiplicity distribution (Figure 2(b) and Table 1), we evaluated the systematic terms involving $p^{\rm ch.}_{\rm min.}$ (item 3 in the above list) using the procedure described in [19]: the corrected distribution was parameterized using polynomials, the parameterized distribution was shifted along the multiplicity axis so that its mean coincided with the mean of the standard result, and the systematic uncertainty was defined bin-by-bin by the difference between the shifted and standard distributions.

The uncertainties were added in quadrature to define the total systematic uncertainty. For the differential multiplicity distributions (Figure 2 and Table 1), the systematic uncertainty evaluated for each bin was averaged with the results from its two neighbors to reduce the effect of bin-to-bin fluctuations (the single neighbor was used for bins on the endpoints of the distributions). The largest systematic terms for the $g_{\rm incl.}$ jet measurements were generally found to arise about equally from items 3, 4 and 5 in the above list. The largest systematic terms for the uds jet measurements were generally found to arise from item 3 and, to a lesser extent, from item 1. For the ratios of the gluon to quark jet measurements, the largest systematic terms generally arose from items 1 and 3-5. As an illustration, Table 6 provides a breakdown of the systematic uncertainties evaluated for $\langle n_{\rm ch.}\rangle_{\rm g_{incl.}}$, $\langle n_{\rm ch.}\rangle_{\rm uds\,hemis.}$, and $r_{\rm ch.}$.

From Table 6, it is seen that using the JADE-E0 or cone jet finders to identify the tagged quark jets for the $g_{\rm incl.}$ sample (item 4 in the above list), yields $r_{\rm ch.}=1.488\pm0.024$ (stat.) or $r_{\rm ch.}=1.448\pm0.028$ (stat.), respectively, which differ by less than 2% from the standard result of $r_{\rm ch.}=1.471\pm0.024$ (stat.). This emphasizes that our results are almost independent of the

choice of the jet finding algorithm. In contrast, results for $r_{\rm ch.}$ based on exclusive samples of three-jet $q\bar{q}g$ events vary from $r_{\rm ch.}=1.10 \pm 0.03\,(\mathrm{stat.}+\mathrm{syst.})$ [10] for the cone jet finder to $r_{\rm ch.}=1.37 \pm 0.04\,(\mathrm{stat.}+\mathrm{syst.})$ [32] for the JADE-E0 jet finder and thus exhibit a strong dependence on the jet algorithm employed.

8 Tests of QCD analytic predictions

A number of QCD analytic calculations have been presented for the factorial moments of the multiplicity distributions of separated gluon and quark jets. Our data permit a test of these calculations for the first time. In the following, we test the predictions of analytic calculations for the cumulant moments K_q. We study K_q moments, rather than F_q moments, since the results for different ranks q are largely independent of each other as was discussed in section 7.2.

An early calculation [4], valid to the next-to-leading order (n.l.o.) of perturbation theory, expresses its results in terms of the strong coupling strength, α_S, and the number of active quark flavors in the parton shower, n_f, allowing the theoretical sensitivity to these quantities to be tested. This calculation does not incorporate energy conservation into the parton branching processes. More recently, a calculation [5] has been presented which is exact for a fixed value of α_S and valid to the next-to-next-to-leading order (n.n.l.o.) if the coupling strength is allowed to run. In this paper, we refer to this result as the "n.n.l.o." calculation. By "exact", it is meant that the QCD evolution equation is solved without resorting to a perturbative expansion. Energy conservation, but not momentum conservation, is included in the n.n.l.o. result (angular-ordering of partons, introduced to partially account for coherence effects, results in approximate momentum conservation [28]). The n.n.l.o. results are presented for a fixed value of the coupling strength, α_S=0.22. This value is intended to be an "effective" one, appropriate to account for realistic running of α_S in the parton evolution of Z^0 decays. The number of active quark flavors is assumed to be n_f=4. Therefore, unlike the n.l.o. calculation, the n.n.l.o. calculation has not yet been presented in a form which allows the values of α_S and n_f to be varied. The results of the n.n.l.o. calculation are not believed to be strongly dependent on the choice of α_S or n_f or on the use of a fixed α_S value rather than a running value, however [27, 28].

In Figures 8 and 9, we present the predictions of the analytic calculations for the K_q moments in comparison to our measurements from Figure 6. The results are shown for gluon jets in Figure 8 and for quark jets in Figure 9. Besides the n.l.o. and n.n.l.o. results, we show the leading order (l.o.) results, obtained from the n.l.o. equations by dropping the n.l.o. correction terms. The n.l.o. formulae are evaluated under three conditions: (1) n_f=5 and $\Lambda_{\overline{\rm MS}}^{(n_f=5)} = 0.209$ GeV [23], (2) n_f=3 and $\Lambda_{\overline{\rm MS}}^{(n_f=3)} = 0.340$ GeV, for which $\Lambda_{\overline{\rm MS}}^{(n_f=3)}$ is derived from $\Lambda_{\overline{\rm MS}}^{(n_f=5)}$ using the prescription relating $\Lambda_{\overline{\rm MS}}^{(n_f=3)}$ to $\Lambda_{\overline{\rm MS}}^{(n_f=5)}$ given in [33], and (3) n_f=5 and $\Lambda_{\overline{\rm MS}}^{(n_f=5)} = 0.209$ GeV, with the energy scale at which α_S is evaluated reduced from $E_{\rm c.m.}$ to $E_{\rm c.m.}/4$.[8] We take the midpoint between the extreme values found using these three conditions as the central n.l.o. result, and define a theoretical uncertainty by taking the difference between the central and extreme values: the extreme values are in all cases given by condition (1), which yields the maximum predicted values of K_q at n.l.o., and (2), which yields the minimum

[8] This choice of energy scales is taken from [34].

predicted values.

From Figures 8 and 9, it is seen that the predictions of the l.o. calculation (the star symbols) are always well in excess of the data. It is seen that large negative corrections are introduced at n.l.o. (the asterisk symbols with uncertainties in Figures 8 and 9), which bring the theory into agreement with the data for q=2, but which result in even larger discrepancies between data and theory for q=4 and q=5 than are observed at l.o. In contrast, the n.n.l.o. calculation (the triangle symbols in Figures 8 and 9) is seen to provide a reasonable qualitative description of the gluon and quark jet results for all q values. There remain important numerical discrepancies between the n.n.l.o. predictions and our data: the n.n.l.o. results for K_q are 0.14, 0.029, 0.0051 and -0.00042 for gluon jets and 0.32, 0.18, 0.12 and 0.065 for quark jets [5], for ranks q=2, 3, 4 and 5, respectively. For q=2 and 3, these results are typically a factor of 3 to 6 larger than the experimental results given in Tables 2 and 3; for q=4 and 5, the discrepancies are in some cases larger and in some cases smaller than this. Nonetheless, it is apparent from Figures 8 and 9 that the n.n.l.o. results represent a striking improvement in the theoretical description of the cumulant moment data in comparison to the results provided by the lower order calculations. This suggests that higher order corrections and energy conservation are essential to obtain a reasonable analytic description of gluon and quark jet multiplicity data, similar to what we observed in our study of the mean multiplicity ratio $r_{\rm ch.}$ [3].

Although the analytic calculations do not provide an accurate quantitative description of the gluon and quark jet moments, it can be anticipated that certain factors, such as hadronization and the dependence of the predictions on n_f or the energy scale, will be common to the gluon and quark jet results. Therefore, in Figure 7, we show the analytic predictions for the ratios r_{K_q}, defined in section 7.2. For purposes of comparison, the parton level predictions of Herwig and Jetset are shown as well. It is seen that the three analytic results, valid to l.o., n.l.o. and n.n.l.o., yield almost identical results for r_{K_q}. This agreement, in stark contrast to the very different predictions which the calculations provide for the individual gluon and quark jet moments (Figures 8 and 9), suggests that the theoretical uncertainties of r_{K_q} are small, and in particular that these ratios are only weakly sensitive to the effect of energy conservation and to the values of α_S and n_f. The theoretical uncertainties evaluated for the n.l.o. results are seen to be much larger than the experimental uncertainties in Figures 8 and 9, but much smaller than the experimental uncertainties in Figure 7, which supports this conclusion.

For q=2, the analytic calculations predict that the K_q moment of gluon jets is smaller than the corresponding moment of quark jets by a factor of about 2.3 (Figure 7). For higher ranks, the difference between the gluon and quark jet moments is predicted to be even larger. These results are in good agreement with our measurements, as is seen from Figure 7.

Comparing the r_{K_q} results of Herwig and Jetset at the parton and hadron levels (i.e. comparing the open circle symbols to the dashed horizontal lines and the square symbols to the solid horizontal lines in Figure 7), it is seen that the hadronization corrections predicted by the models are not negligible, especially for q=2 and q=3. The interpretation of the parton level Monte Carlo predictions is somewhat unclear, however, for two reasons. First, the Monte Carlo simulations implement cutoffs, denoted Q_0, to truncate the parton shower at small parton invariant masses. For Herwig and Jetset, $Q_0 \sim 1$ GeV. We find the parton level Monte Carlo results for r_{K_q} to be sensitive to Q_0. In contrast, analytic predictions for r_{K_q} do not depend on a cutoff and in this sense are more reliable theoretically. Second, the mean numbers of partons

present at the end of the perturbative shower are small for the Monte Carlo results shown in Figure 7: an average of only 4.6 and 2.9 partons are present, respectively, for 41.8 GeV gluon and uds quark jet hemispheres generated using Herwig with our tuned parameter set. The corresponding results for Jetset are 4.1 and 2.9. These small numbers make it questionable whether the parton level Monte Carlo predictions for r_{K_q} have much numerical meaning. To further investigate this question, we used Herwig to generate 5 TeV gg and uds $q\overline{q}$ hemisphere jets: the resulting mean number of partons present at the end of the perturbative shower was 56.7 for gluon jets and 30.2 for quark jets. The 5 TeV Monte Carlo jets avoid the two problems mentioned above for 41.8 GeV Monte Carlo jets: the condition $E_{\rm jet} >> Q_0$ effectively eliminates the dependence of the parton level predictions on Q_0, while the large parton multiplicities make calculation of higher factorial and cumulant moments numerically sensible. The ratios r_{K_q} determined using the simulated 5 TeV jets were found to be in good agreement with the analytic results shown in Figure 7 at both the parton and hadron levels. We conclude that the hadronization corrections predicted by the simulations for 41.8 GeV jets are numerically questionable and that the agreement between the data and analytic calculations shown in Figure 7 is probably not coincidental.

The OPAL results are based on event hemispheres. The n.n.l.o. results are based on the full event multiplicity distributions (in contrast, the definitions employed for the n.l.o. calculation correspond to hemispheres [35]). To assess the effect of this difference, we used Herwig and Jetset to evaluate the K_q moments of the full event charged particle multiplicity distributions. The full event results were compared to the corresponding hemisphere results shown in Figures 6 and 7. Use of full events rather than hemispheres was found to reduce the magnitude of the gluon and quark jet K_q moments, typically by 30-60%, further increasing the quantitative discrepancy between the data and n.n.l.o. calculation. This difference does not affect the qualitative agreement between the data and n.n.l.o. calculation exhibited in Figures 8 and 9 since the visible positions of the data are already near zero on the scales of those figures. The effect of the difference between hemispheres and full events was found to be negligible for the ratios r_{K_q} shown in Figure 7.

9 Summary and conclusion

In this study, we have presented measurements of the multiplicity distributions of gluon and quark jets. We have determined their mean, dispersion, skew and curtosis values, and factorial and cumulant moments. The gluon and quark jets are defined by inclusive sums over the particles in $\rm g_{incl.}$ and uds event hemispheres, respectively, with the $\rm g_{incl.}$ gluon jet opposite to a hemisphere containing two identified quark jets in $\rm e^+e^-$ annihilations (the quark jets for the $\rm g_{incl.}$ identification are defined using a jet finding algorithm). These inclusive definitions are in close correspondence to the definition of jets used for QCD analytic calculations, allowing a meaningful comparison of data with theory. Our results for the gluon jet properties are almost independent of the choice of the jet finding algorithm, in contrast to other studies of high energy ($E_{\rm jet}>$ 5 GeV) gluon jets. The energy of the jets in our study is about 42 GeV.

We find the mean multiplicity values of gluon and quark jets to differ by about 50%, in agreement with our earlier result [3] but with a substantially reduced uncertainty. We also observe differences between the gluon and quark jet skew and curtosis values: the multiplicity

distribution of quark jets is observed to be about twice as skewed (asymmetric) as the multiplicity distribution of gluon jets, while quark jets are found to have a larger curtosis value (curtosis measures the deviation of a distribution from a gaussian shape) than gluon jets. The dispersions of gluon and quark jets are found to be the same to within the experimental uncertainties. These results are well reproduced by the predictions of QCD parton shower event generators.

We analyze the gluon and quark jet distributions to determine their normalized factorial and cumulant factorial moments. These measurements are used to perform the first test of QCD analytic predictions of these moments for separated gluon and quark jets. We base our test of the analytic results on the cumulant factorial moments, K_q, since we observe that K_q moments of different rank q are largely uncorrelated with each other, unlike the factorial moments, F_q. A recent next-to-next-to-leading order calculation which includes energy conservation [5] is found to provide a a striking improvement in the theoretical description of the individual gluon and quark jet K_q values, in comparison to the description provided by the leading and next-to-leading order calculations.

Our analysis of the K_q moments reveals large differences between gluon and quark jets. For rank q=2, the ratio of the cumulant moments of gluon to quark jets is found to be r_{K_2}=0.30 $\pm$ 0.11 (stat.) $\pm$ 0.13 (syst.). For rank q=3, r_{K_3}=0.04 $\pm$ 0.15 (stat.) $\pm$ 0.18 (syst.). The analytic predictions for r_{K_q} are found to be in quantitative agreement with the data.

10 Acknowledgements

We wish to thank the SL Division for the efficient operation of the LEP accelerator and for their continuing close cooperation with our experimental group. We thank our colleagues from CEA, DAPNIA/SPP, CE-Saclay for their efforts over the years on the time-of-flight and trigger systems which we continue to use. In addition to the support staff at our own institutions we are pleased to acknowledge the:

Department of Energy, USA,
National Science Foundation, USA,
Particle Physics and Astronomy Research Council, UK,
Natural Sciences and Engineering Research Council, Canada,
Israel Science Foundation, administered by the Israel Academy of Science and Humanities,
Minerva Gesellschaft,
Benoziyo Center for High Energy Physics,
Japanese Ministry of Education, Science and Culture (the Monbusho) and a grant under the Monbusho International Science Research Program,
German Israeli Bi-national Science Foundation (GIF),
Bundesministerium für Bildung, Wissenschaft, Forschung und Technologie, Germany,
National Research Council of Canada,
Hungarian Foundation for Scientific Research, OTKA T-016660, T023793 and OTKA F-023259.

References

[1] CLEO Collaboration, M. S. Alam *et al.*, Phys. Rev. **D46** (1992) 4822.

[2] J. W. Gary, Phys. Rev. **D49** (1994) 4503.

[3] OPAL Collaboration, G. Alexander *et al.*, Phys. Lett. **B388** (1996) 659.

[4] E. D. Malaza and B. R. Webber, Phys. Lett. **B149** (1984) 501;
E. D. Malaza and B. R. Webber, Nucl. Phys. **B267** (1986) 702.

[5] I. M. Dremin and R. C. Hwa, Phys. Rev. **D49** (1994) 5805;
numerical results for the factorial moment calculation are given in M. Biyajima, I. M. Dremin, V. A. Nechitailo and N. Suzuki, FIAN-TD-97-6 (April 1997), e-Print Archive: hep-ph/9704318.

[6] OPAL Collaboration, K. Ahmet *et al.*, Nucl. Instr. and Meth. **A305** (1991) 275;
P. Allport *et al.*, Nucl. Instr. and Meth. **A324** (1993) 34;
P. Allport *et al.*, Nucl. Instr. and Meth. **A346** (1994) 476.

[7] OPAL Collaboration, G. Alexander *et al.*, Z. Phys. **C69** (1996) 543.

[8] S. Brandt *et al.*, Phys. Lett. **12** (1964) 57;
E. Fahri, Phys. Rev. Lett. **39** (1977) 1587.

[9] S. Catani *et al.*, Phys. Lett. **B269** (1991) 432.

[10] OPAL Collaboration, R. Akers *et al.*, Z. Phys. **C68** (1995) 179.

[11] T. Sjöstrand, Comp. Phys. Comm. **82** (1994) 74.

[12] J. Allison *et al.*, Nucl. Instr. and Meth. **A317** (1992) 47.

[13] OPAL Collaboration, P.D. Acton *et al.*, Z. Phys. **C58** (1993) 387.

[14] J. W. Gary, UCRHEP-E181 (December 1996), e-Print Archive: hep-ex/9701005.

[15] G. Marchesini, B.R. Webber *et al.*, Comp. Phys. Comm. **67** (1992) 465.

[16] JADE Collaboration, W. Bartel *et al.*, Z. Phys. **C33** (1986) 23.

[17] OPAL Collaboration, R. Akers *et al.*, Z. Phys. **C63** (1994) 197.

[18] OPAL Collaboration, P. D. Acton *et al.*, Z. Phys. **C58** (1993) 523.

[19] OPAL Collaboration, P.D. Acton *et al.*, Z. Phys. **C53** (1992) 539.

[20] OPAL Collaboration, R. Akers *et al.*, Phys. Lett. **B352** (1995) 176.

[21] A. H. Mueller, Nucl. Phys. **B213** (1983) 85;
A. H. Mueller, Nucl. Phys. **B228** (1983) 351;
B. R. Webber, Phys. Lett. **B143** (1984) 501.

[22] OPAL Collaboration, K. Ackerstaff *et al.*, CERN-PPE-97-015 (February 1997).

[23] R. M. Barnett *et al.*, "Review of Particle Physics", Phys. Rev. **D54** (1996) 1.

[24] OPAL Collaboration, G. Alexander *et al.*, Z. Phys. **C72** (1996) 191.

[25] I. M. Dremin and R. C. Hwa, Phys. Lett. **B324** (1994) 477;
I. M. Dremin and V. A. Nechitailo, Modern Phys. Lett. **A9** (1994) 1471.

[26] A. Bialas and R. Peschanski, Nucl. Phys. **B273** (1986) 703.

[27] For reviews, see I. M. Dremin, Physics-Uspekhi **37**(8) (1994) 715;
E. A. de Wolf, I. M. Dremin and W. Kittel, Phys. Rep. **270** (1996) 1.

[28] I. M. Dremin, private communication.

[29] SLD Collaboration, K. Abe *et al.*, Phys. Lett. **B371** (1996) 149.

[30] V. Arena *et al.*, Phys. Lett. **B336** (1994) 119.

[31] See, for example, R. Barlow, Manchester preprint MAN/HEP/93/9 (April 1994).

[32] DELPHI Collaboration, P. Abreu *et al.*, Z. Phys. **C70** (1996) 179.

[33] W. Bernreuther, Annals of Physics **151** (1983) 127.

[34] Z. Kunszt, P. Nason *et al.*, Z Physics at LEP 1, Vol. 1, CERN 89-08, eds. G. Altarelli, R. Kleiss and C. Verzegnassi, Geneva 1989.

[35] B. R. Webber, private communication.

$n_{\mathrm{ch.}}$	$\mathrm{P}(n_{\mathrm{ch.}})$, $\mathrm{g}_{\mathrm{incl.}}$ jets (%)	$\mathrm{P}(n_{\mathrm{ch.}})$, uds jets (%)
0	—	$0.040 \pm 0.006 \pm 0.027$
1	—	$0.182 \pm 0.011 \pm 0.068$
2	—	$0.726 \pm 0.023 \pm 0.099$
3	—	$1.74 \pm 0.03 \pm 0.18$
4	$0.31 \pm 0.20 \pm 0.38$	$3.64 \pm 0.05 \pm 0.20$
5	$0.86 \pm 0.44 \pm 0.43$	$5.59 \pm 0.05 \pm 0.25$
6	$1.24 \pm 0.63 \pm 0.68$	$8.12 \pm 0.07 \pm 0.26$
7	$2.08 \pm 0.85 \pm 0.77$	$9.41 \pm 0.06 \pm 0.23$
8	$3.9 \pm 1.0 \pm 1.0$	$10.54 \pm 0.07 \pm 0.26$
9	$5.2 \pm 1.3 \pm 0.9$	$10.08 \pm 0.07 \pm 0.24$
10	$6.5 \pm 1.4 \pm 0.9$	$9.57 \pm 0.07 \pm 0.27$
11	$7.0 \pm 1.3 \pm 1.1$	$8.21 \pm 0.06 \pm 0.20$
12	$7.7 \pm 1.6 \pm 1.0$	$7.06 \pm 0.06 \pm 0.19$
13	$9.0 \pm 1.5 \pm 1.1$	$5.69 \pm 0.05 \pm 0.12$
14	$9.4 \pm 1.5 \pm 0.8$	$4.64 \pm 0.06 \pm 0.10$
15	$9.4 \pm 1.5 \pm 1.0$	$3.637 \pm 0.042 \pm 0.075$
16	$8.7 \pm 1.5 \pm 1.0$	$2.858 \pm 0.036 \pm 0.081$
17	$7.2 \pm 1.4 \pm 1.1$	$2.195 \pm 0.034 \pm 0.090$
18	$5.6 \pm 1.1 \pm 1.2$	$1.688 \pm 0.030 \pm 0.077$
19	$4.6 \pm 1.1 \pm 1.1$	$1.254 \pm 0.027 \pm 0.062$
20	$3.2 \pm 0.9 \pm 1.0$	$0.932 \pm 0.023 \pm 0.045$
21	$2.38 \pm 0.90 \pm 0.68$	$0.672 \pm 0.019 \pm 0.046$
22	$1.55 \pm 0.71 \pm 0.46$	$0.477 \pm 0.016 \pm 0.062$
23	$1.08 \pm 0.81 \pm 0.48$	$0.342 \pm 0.013 \pm 0.070$
24	$0.81 \pm 0.58 \pm 0.64$	$0.241 \pm 0.011 \pm 0.058$
25	$1.23 \pm 0.52 \pm 0.84$	$0.167 \pm 0.010 \pm 0.034$
26	$0.27 \pm 0.30 \pm 0.86$	$0.113 \pm 0.007 \pm 0.017$
27	$0.66 \pm 0.32 \pm 0.57$	$0.074 \pm 0.006 \pm 0.013$
28	—	$0.050 \pm 0.004 \pm 0.010$
29	$0.05 \pm 0.14 \pm 0.18$	$0.0311 \pm 0.0035 \pm 0.0088$
30	$0.15 \pm 0.09 \pm 0.15$	$0.0222 \pm 0.0029 \pm 0.0066$
31	—	$0.0130 \pm 0.0020 \pm 0.0059$
32	—	$0.0091 \pm 0.0016 \pm 0.0039$
33	—	$0.0039 \pm 0.0012 \pm 0.0029$
34	—	$0.0024 \pm 0.0011 \pm 0.0016$
35	—	$0.0016 \pm 0.0008 \pm 0.0012$
36	—	$0.00056 \pm 0.00039 \pm 0.00077$

Table 1: Charged particle multiplicity distributions, expressed in per cent (%), of 41.8 GeV $\mathrm{g}_{\mathrm{incl.}}$ gluon jets and 45.6 GeV uds quark jets. The first uncertainty is statistical and the second is systematic. The statistical and systematic uncertainties are correlated between bins.

q	F_q	K_q	H_q
2	$1.023 \pm 0.008 \pm 0.011$	$0.0233 \pm 0.0083 \pm 0.0109$	$0.0228 \pm 0.0078 \pm 0.0104$
3	$1.071 \pm 0.026 \pm 0.034$	$0.0010 \pm 0.0039 \pm 0.0048$	$0.0009 \pm 0.0035 \pm 0.0045$
4	$1.146 \pm 0.059 \pm 0.074$	$0.0000 \pm 0.0023 \pm 0.0015$	$0.0000 \pm 0.0019 \pm 0.0013$
5	$1.25 \pm 0.11 \pm 0.13$	$-0.0005 \pm 0.0018 \pm 0.0014$	$-0.0004 \pm 0.0013 \pm 0.0011$

Table 2: The F_q, K_q and H_q factorial moments of the charged particle multiplicity distribution of 41.8 GeV $g_{\rm incl.}$ gluon jets. The first uncertainty is statistical and the second is systematic.

q	F_q	K_q	H_q
2	$1.0820 \pm 0.0006 \pm 0.0046$	$0.0820 \pm 0.0006 \pm 0.0048$	$0.0758 \pm 0.0005 \pm 0.0041$
3	$1.275 \pm 0.002 \pm 0.017$	$0.0291 \pm 0.0006 \pm 0.0035$	$0.0228 \pm 0.0004 \pm 0.0026$
4	$1.637 \pm 0.005 \pm 0.042$	$0.0081 \pm 0.0007 \pm 0.0015$	$0.00496 \pm 0.00043 \pm 0.00089$
5	$2.274 \pm 0.014 \pm 0.093$	$-0.00300 \pm 0.00096 \pm 0.00095$	$-0.00132 \pm 0.00043 \pm 0.00044$

Table 3: The F_q, K_q and H_q factorial moments of the charged particle multiplicity distribution of 45.6 GeV uds quark jets. The first uncertainty is statistical and the second is systematic.

	$\langle n_{\rm ch.}\rangle$	D	γ	c	F_2	F_3	F_4	F_5	K_2	K_3	K_4	K_5
$\langle n_{\rm ch.}\rangle$	1.00	0.22	0.13	0.03	−0.03	−0.01	0.01	0.01	−0.03	0.13	−0.06	−0.07
D		1.00	0.36	0.14	0.97	0.96	0.94	0.90	0.97	0.36	−0.02	−0.14
γ			1.00	0.77	0.33	0.46	0.57	0.66	0.33	0.99	0.42	−0.18
c				1.00	0.14	0.24	0.36	0.48	0.14	0.78	0.90	0.08
F_2					1.00	0.99	0.96	0.92	1.00	0.33	−0.01	−0.13
F_3						1.00	0.99	0.96	0.99	0.46	0.06	−0.15
F_4							1.00	0.99	0.96	0.58	0.15	−0.15
F_5								1.00	0.92	0.67	0.26	−0.13
K_2									1.00	0.33	−0.01	−0.13
K_3										1.00	0.43	−0.19
K_4											1.00	0.25
K_5												1.00

Table 4: Correlation matrix between the mean $\langle n_{\rm ch.}\rangle$, dispersion D, skew γ, curtosis c, and the F_q and K_q factorial moments of the charged particle multiplicity distribution, for 41.8 GeV $g_{\rm incl.}$ gluon jets obtained using the Jetset Monte Carlo at the generator level. Boxes have been drawn around correlation coefficients which have magnitudes of 0.90 or larger.

q	r_{F_q}	r_{K_q}	r_{H_q}
2	$0.949 \pm 0.008 \pm 0.011$	$0.30 \pm 0.11 \pm 0.13$	$0.32 \pm 0.11 \pm 0.14$
3	$0.850 \pm 0.021 \pm 0.026$	$0.04 \pm 0.15 \pm 0.18$	$0.05 \pm 0.17 \pm 0.22$
4	$0.716 \pm 0.037 \pm 0.040$	$0.00 \pm 0.33 \pm 0.22$	$-0.01 \pm 0.44 \pm 0.31$
5	$0.571 \pm 0.051 \pm 0.054$	$0.15 \pm 0.61 \pm 0.43$	$0.27 \pm 0.96 \pm 0.72$

Table 5: The ratios r_{F_q}, r_{K_q} and r_{H_q} of the F_q, K_q and H_q factorial moments of 41.8 GeV $\mathrm{g_{incl.}}$ gluon and uds quark jets. The first uncertainty is statistical and the second is systematic.

	$\langle n_{\mathrm{ch.}} \rangle_{\mathrm{g\,incl.}}$	$\langle n_{\mathrm{ch.}} \rangle_{\mathrm{uds\,hemis.}}$	$r_{\mathrm{ch.}}$
1. Charged tracks only	-0.13	$+0.05$	-0.020
2. Herwig corrections	-0.10	$+0.01$	-0.012
3. $p > 0.20$ GeV/c	-0.15	-0.17	$+0.010$
($\lvert\cos(\theta_{\mathrm{particle}})\rvert < 0.70$	-0.10	-0.04	-0.004)
4. Cone jet finder	-0.23	——	-0.023
(JADE-E0 jet finder	$+0.17$	——	$+0.018$)
5. $\theta_{\mathrm{jet\,a-thrust}}, \theta_{\mathrm{jet\,b-thrust}} < 65^\circ$	$+0.21$	——	$+0.022$
($\theta_{\mathrm{jet\,a-jet\,b}} > 65^\circ$	$+0.19$	——	$+0.020$)
6. One track with $b/\sigma_b > 2.5$	$+0.04$	——	$+0.004$
7. On-peak data only	-0.11	——	-0.011
8. 70° cone	——	-0.01	$+0.002$
9. $b/\sigma_b > 2.5$	——	-0.02	$+0.003$
10. Uncertainty of $\langle E \rangle_{\mathrm{g\,incl.}}$	——	——	± 0.008
(Energy correction factor	——	——	± 0.004)
Total systematic uncertainty	0.40	0.18	0.043

Table 6: Differences between the results of the standard analysis and those found by repeating the analysis with the systematic changes listed, for the mean charged particle multiplicity value $\langle n_{\mathrm{ch.}} \rangle$ of 41.8 GeV $\mathrm{g_{incl.}}$ gluon jets, for the $\langle n_{\mathrm{ch.}} \rangle$ value of 45.6 GeV uds quark jets, and for the ratio $r_{\mathrm{ch.}}$ between the $\langle n_{\mathrm{ch.}} \rangle$ values of 41.8 GeV $\mathrm{g_{incl.}}$ and uds quark jets. For item 4, "jet a" and "jet b" refer to the two tagged quark jets against which the $\mathrm{g_{incl.}}$ jet recoils and "thrust" refers to the thrust axis. For items 3, 4, 5 and 10, the larger of the two listed differences was assigned as the systematic uncertainty; the smaller of the two differences is given in parentheses for purposes of information.

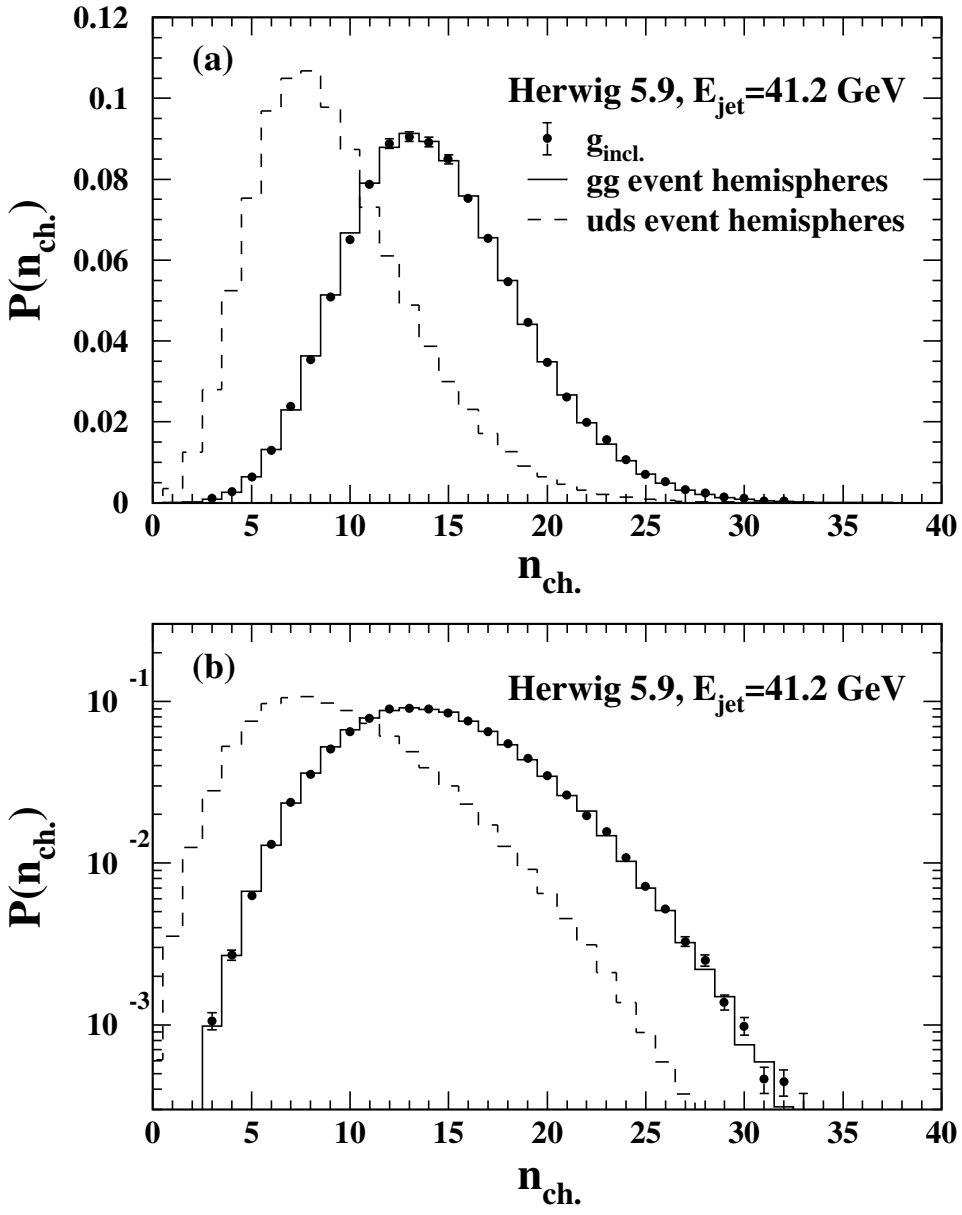

Figure 1: The prediction of the Herwig parton shower event generator for the charged particle multiplicity distribution of $g_{\,\mathrm{incl.}}$ gluon jets from e^+e^- annihilations, in comparison to the Herwig prediction for gg and uds event hemispheres: (a) on a linear scale, and (b) on a logarithmic scale. The jet energies are 41.2 GeV, corresponding to a c.m. energy of 91.2 GeV for the generation of the $e^+e^- \to q\overline{q}\,g_{\,\mathrm{incl.}}$ events.

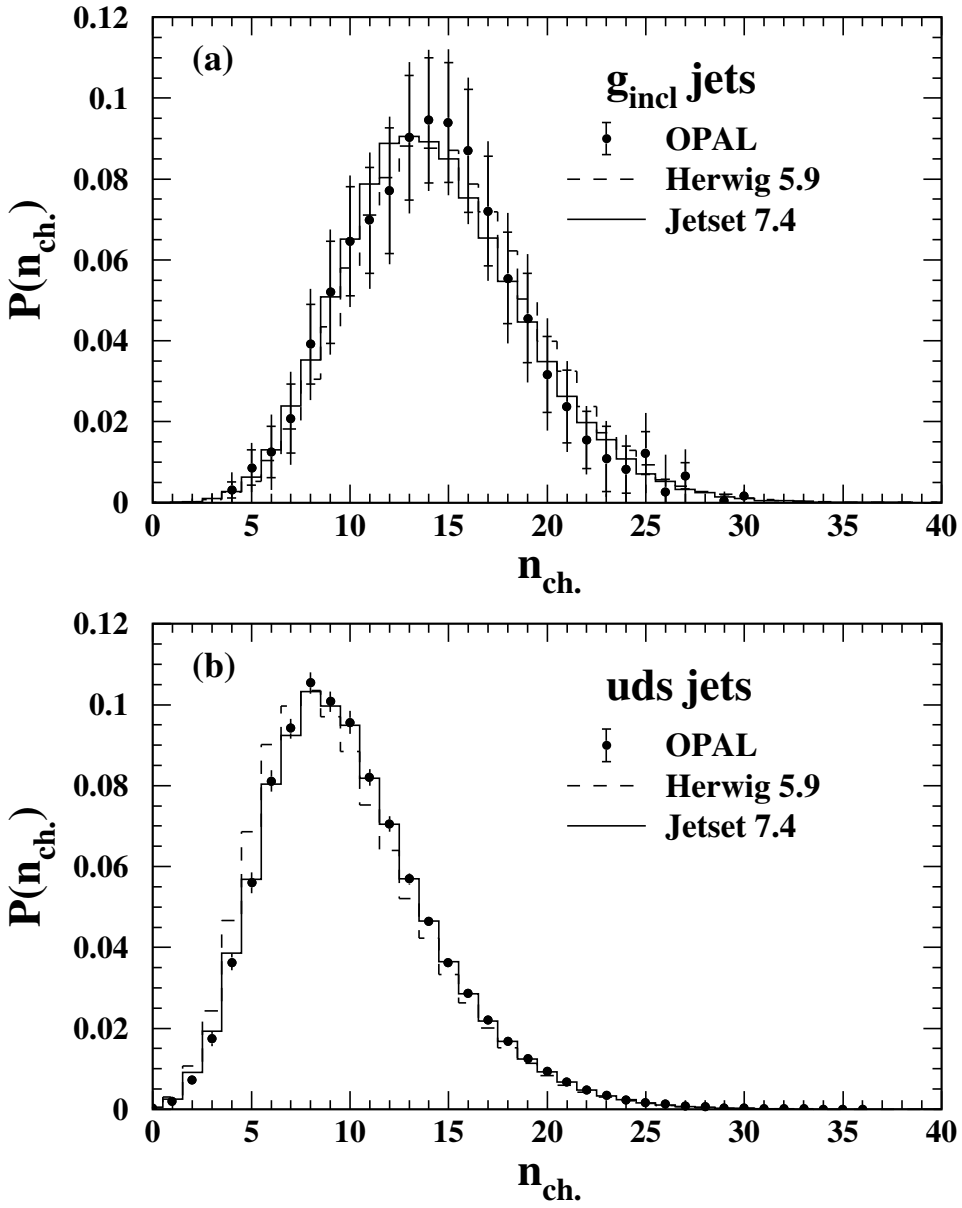

Figure 2: Corrected distributions of charged particle multiplicity for (a) 41.8 GeV $g_{incl.}$ gluon jets, and (b) 45.6 GeV uds quark jets. The total uncertainties are shown by vertical lines. The statistical uncertainties are indicated by small horizontal bars. (The statistical uncertainties are too small to be seen for the uds jets.) The uncertainties are correlated between bins. The predictions of the Herwig and Jetset parton shower event generators are also shown. Numerical values for these data are given in Table 1.

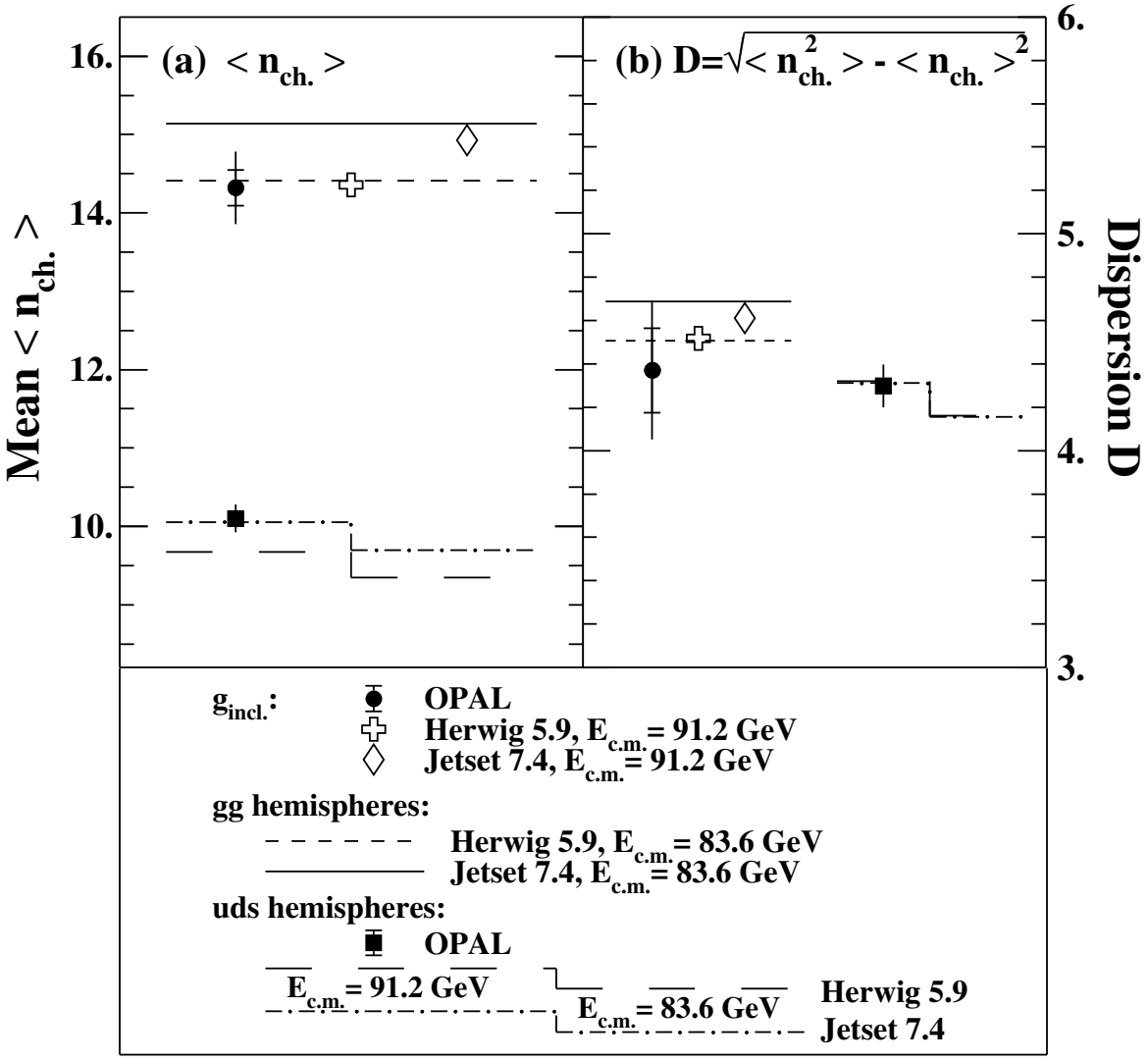

Figure 3: (a) The mean, $\langle n_{\,\mathrm{ch.}}\rangle$, and (b) the dispersion, D, of the charged particle multiplicity distribution of 41.8 GeV $\mathrm{g}_{\,\mathrm{incl.}}$ gluon jets and 45.6 GeV uds quark jets. The total uncertainties are shown by vertical lines. The statistical uncertainties are indicated by small horizontal bars. (The statistical uncertainties are too small to be seen for the uds jets.) The predictions of the Herwig and Jetset parton shower event generators are also shown.

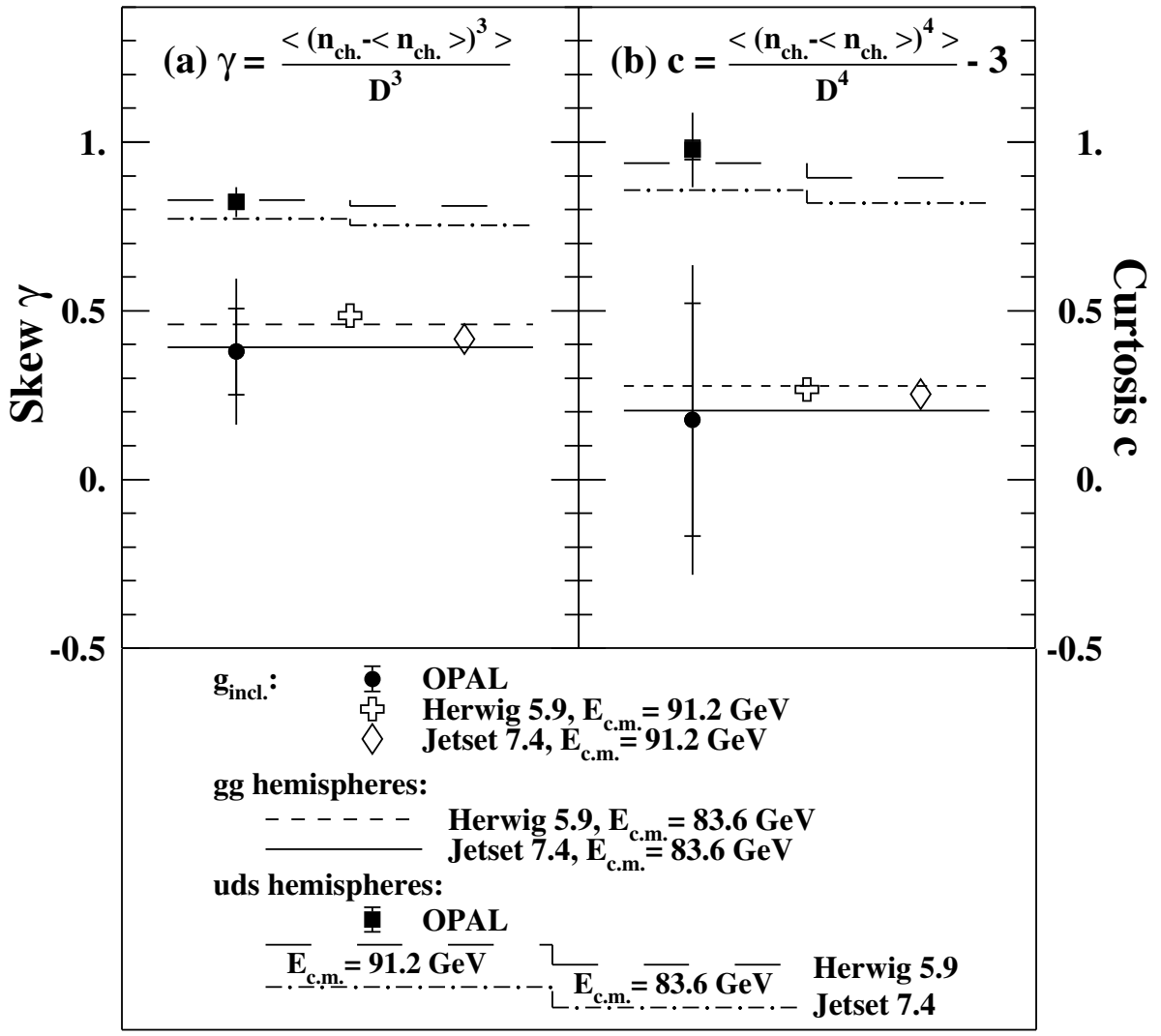

Figure 4: (a) The skew, γ, and (b) the curtosis, c, of the charged particle multiplicity distribution of 41.8 GeV $g_{incl.}$ gluon jets and 45.6 GeV uds quark jets. The total uncertainties are shown by vertical lines. The statistical uncertainties are indicated by small horizontal bars. (The statistical uncertainties are too small to be seen for the uds jets.) The predictions of the Herwig and Jetset parton shower event generators are also shown.

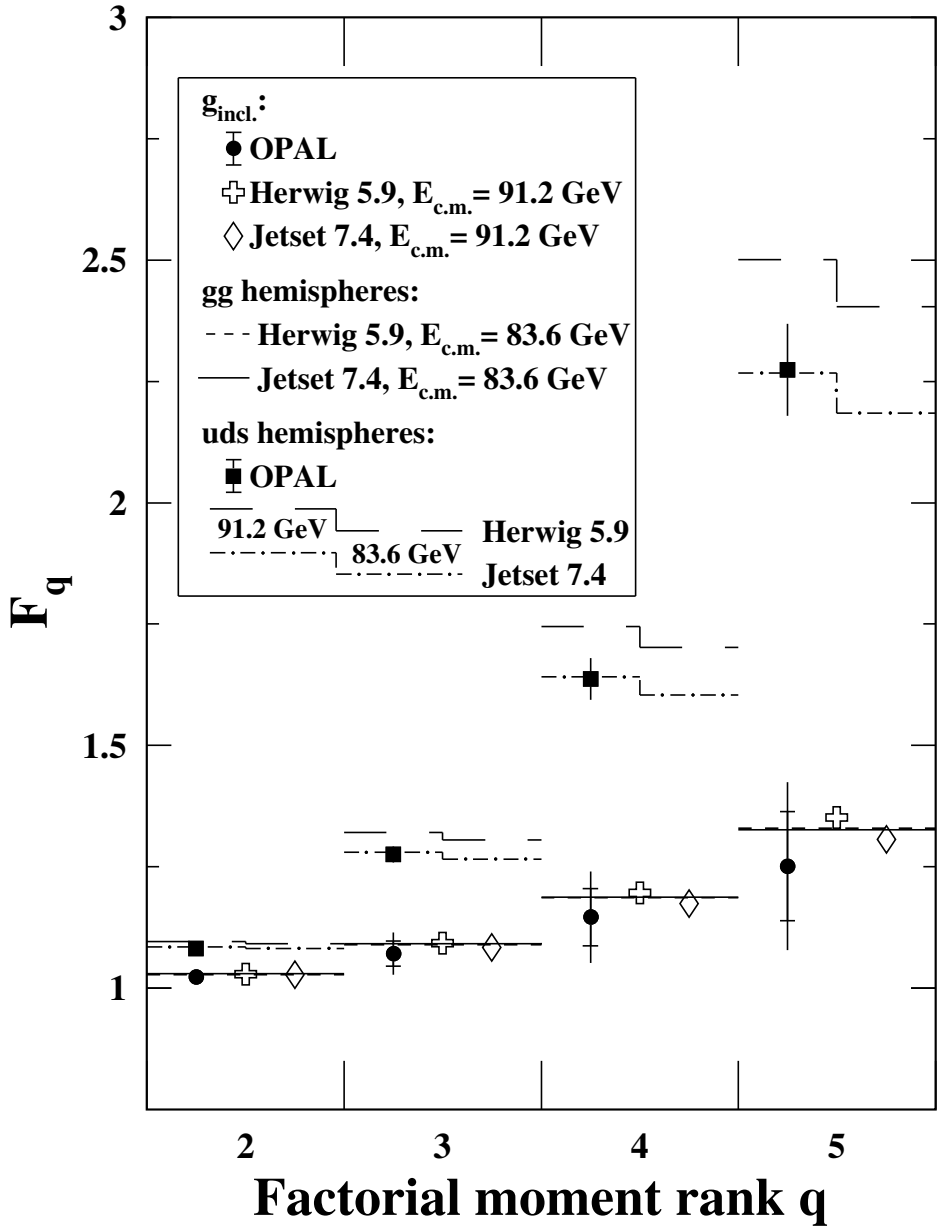

Figure 5: The normalized factorial moments of the charged particle multiplicity distribution, F_q, for 41.8 GeV $g_{incl.}$ gluon jets and 45.6 GeV uds quark jets. The total uncertainties are shown by vertical lines. The statistical uncertainties are indicated by small horizontal bars. (The statistical uncertainties are too small to be seen for the uds jets.) The predictions of the Herwig and Jetset parton shower event generators are also shown.

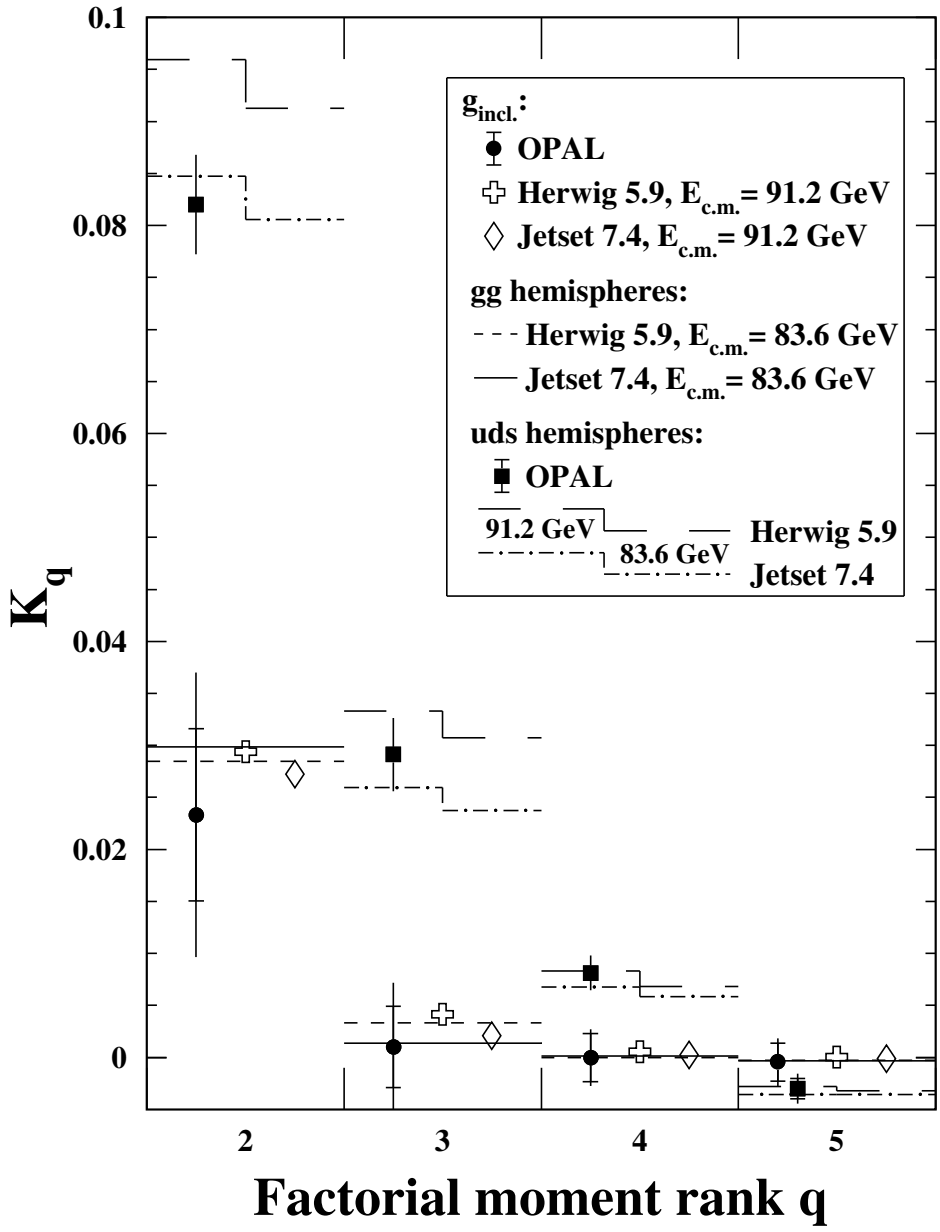

Figure 6: The cumulant factorial moments of the charged particle multiplicity distribution, K_q, for 41.8 GeV $g_{incl.}$ gluon jets and 45.6 GeV uds quark jets. The total uncertainties are shown by vertical lines. The statistical uncertainties are indicated by small horizontal bars. (The statistical uncertainties are too small to be seen for the uds jets.) The predictions of the Herwig and Jetset parton shower event generators are also shown.

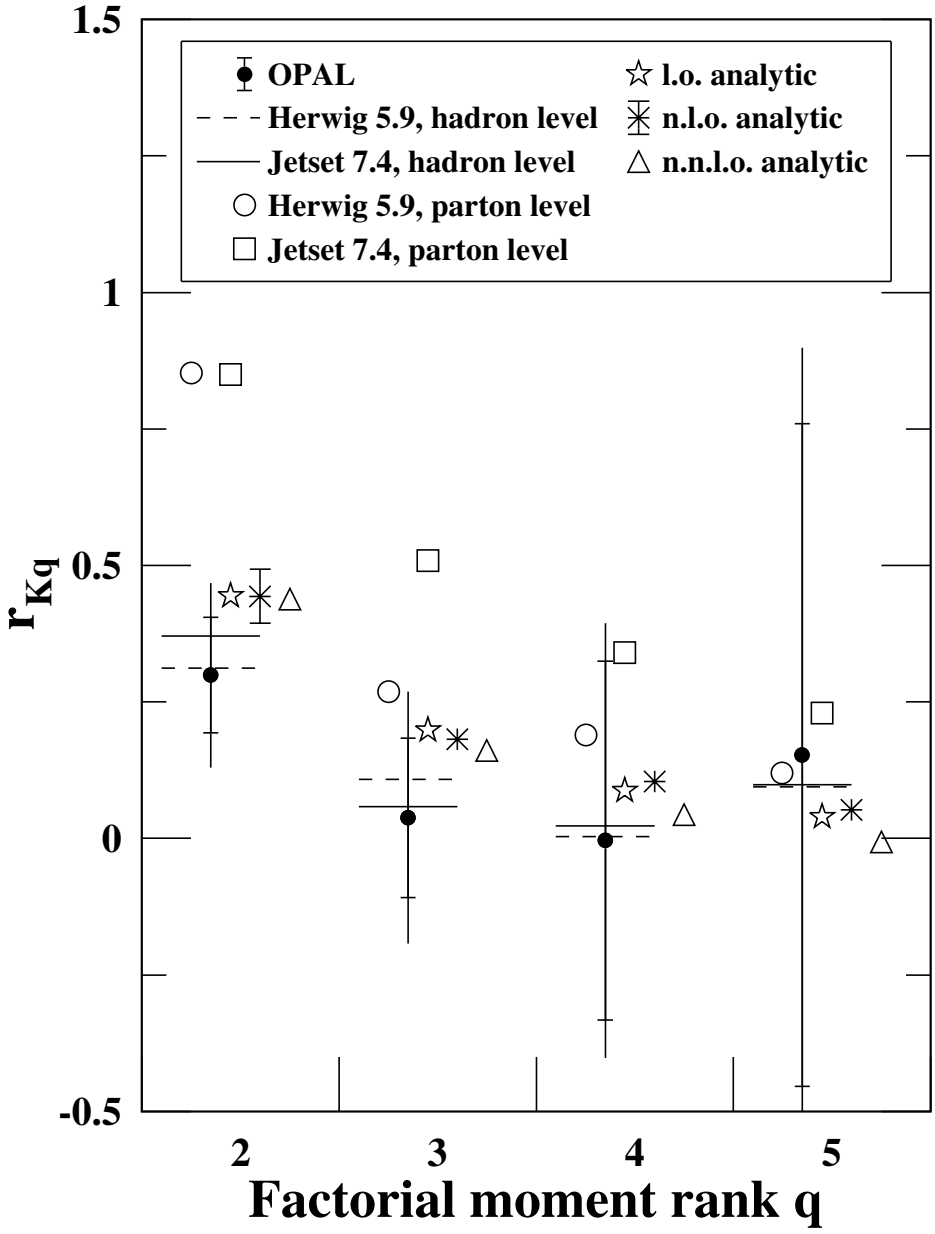

Figure 7: The ratios r_{K_q} of the cumulant factorial moments K_q of 41.8 GeV gluon and quark jets, in comparison to the predictions of QCD analytic calculations and the Herwig and Jetset parton shower event generators. The total uncertainties of the data are shown by vertical lines. The experimental statistical uncertainties are indicated by small horizontal bars. The uncertainties evaluated for the n.l.o. analytic calculation are described in the text.

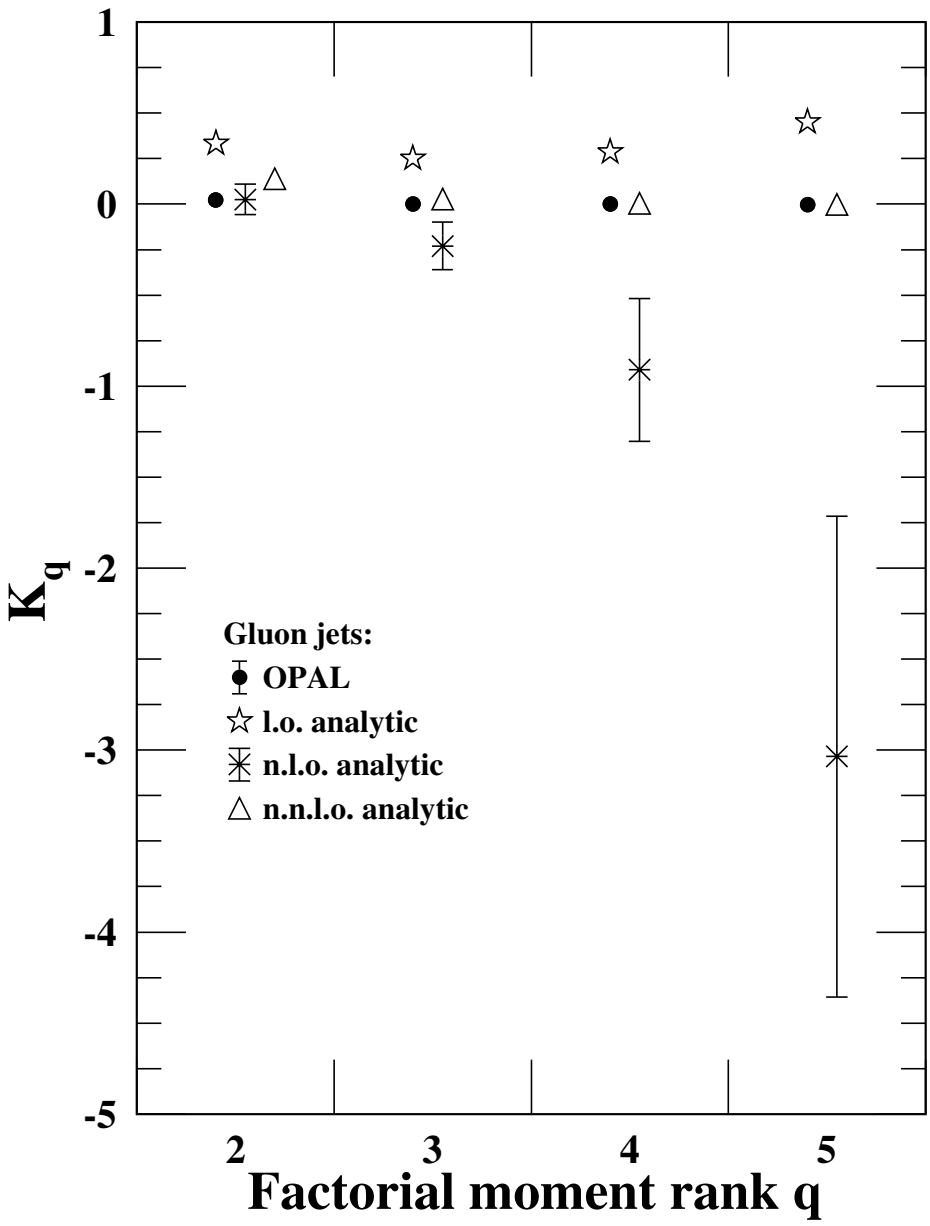

Figure 8: Analytic predictions for the cumulant factorial moments, K_q, of gluon jets, in comparison to the OPAL measurements. The uncertainties evaluated for the n.l.o. analytic calculation are described in the text.

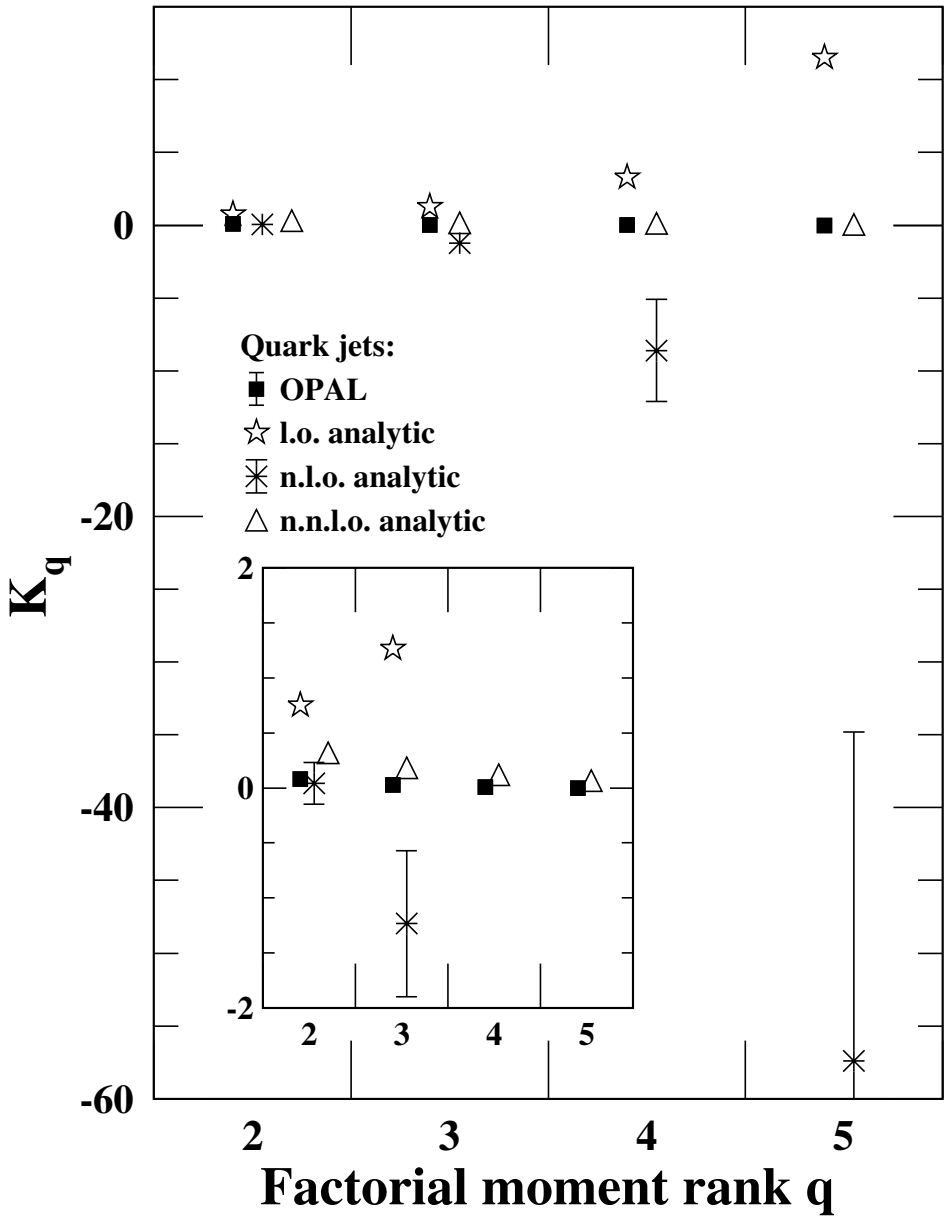

Figure 9: Analytic predictions for the cumulant factorial moments, K_q, of quark jets, in comparison to the OPAL measurements. The inset shows an expanded view. The uncertainties evaluated for the n.l.o. analytic calculation are described in the text.